Gap equations at inhomogeneous phases in the Nambu–Jona-Lasinio model

Gap Gleichungen in inhomogenen Phasen im Nambu–Jona-Lasinio Modell
Master-Thesis von Eduard Alert
Tag der Einreichung:

1. Gutachten: PD Dr. Michael Buballa
2. Gutachten: Prof. Dr. Jens Braun

TECHNISCHE
UNIVERSITÄT
DARMSTADT

Institut für Kernphysik
Theoretische Kernphysik
NHQ

Gap equations at inhomogeneous phases in the Nambu–Jona-Lasinio model
Gap Gleichungen in inhomogenen Phasen im Nambu–Jona-Lasinio Modell

Vorgelegte Master-Thesis von Eduard Alert

1. Gutachten: PD Dr. Michael Buballa
2. Gutachten: Prof. Dr. Jens Braun

Tag der Einreichung:

Erklärung zur Master-Thesis

Hiermit versichere ich, die vorliegende Master-Thesis ohne Hilfe Dritter nur mit den angegebenen Quellen und Hilfsmitteln angefertigt zu haben. Alle Stellen, die aus Quellen entnommen wurden, sind als solche kenntlich gemacht. Diese Arbeit hat in gleicher oder ähnlicher Form noch keiner Prüfungsbehörde vorgelegen.

Darmstadt, den 05. Dezember

(Eduard Alert)

Abstract

In this work we consider spatially dependent condensates in the Nambu–Jona-Lasinio model. As an ansatz for the combination of the scalar and the pseudoscalar condensate in mean-field approximation, we use the finite Fourier series from previous works which is extended by inclusion of higher coefficients and a finite current quark mass. The Fourier amplitudes yield a coupled equation system, which is solved by fixed-point iterations. The solutions of these so-called gap equations lead to sinusoidal modulations, which are compared with each other and with a similar modulation for the chiral condensate.

Zusammenfassung

In dieser Arbeit betrachten wir ortsabhängige Kondensate im Nambu–Jona-Lasinio Modell. Als Ansatz für die Kombination aus skalaren und pseudo-skalaren Kondensat in mean-field Näherung verwenden wir die endliche Fourierentwicklung aus vorherigen Arbeiten und erweitern diese durch Einbeziehung von höheren Koeffizienten und einer endlichen Stromquarkmasse. Die Fourieramplituden ergeben ein gekoppeltes Gleichungssystem, das durch Fixpunktiterationen gelöst wird. Die Lösungen dieser so genannten Gap-Gleichungen führen zu sinusförmigen Modulationen, die miteinander und mit einer ähnlichen Modulation für das chirale Kondensat verglichen werden.

Contents

1 Introduction

The Standard model has been established to explain the fundamental processes of subatomic particles. It includes all actual well-known interactions, except gravity. One of them is the strong interaction which is described by the quantum chromodynamics (QCD) introduced in 1973 to characterize the interactions of quarks and gluons [1]. In contrast to quantum electrodynamics (QED), it has a non-abelian structure, so that the gauge bosons (gluons) can interact with each other because they carry color charges unlike the photons, that are electrically neutral. This leads to three- and four-gluon vertices in perturbation theory.
Quarks occur in six different types of flavor: up, down, charm, strange, top and bottom, which differ in mass and quantum number. These are typically combined to three generations

$$\begin{pmatrix} u \\ d \end{pmatrix}, \begin{pmatrix} c \\ s \end{pmatrix}, \begin{pmatrix} t \\ b \end{pmatrix}. \tag{1.1}$$

The non-abelian structure involves some important properties of the QCD. One of them is the confinement that arises from the strong quark-gluon coupling in the low energy or large distance regime. It states that only color singlet states can exist as free particles. Consequently, free quarks cannot be observed in nature and always appear in colorless bound states, called hadrons. Another feature results from the fact that the quark-gluon coupling becomes weak at high energies or small distances, such that the quarks behave as if they are quasi-free. This is the so called asymptotic freedom discovered by F. Wilczek, D. Gross [2–4] and D. Politzer [5] independently. In this high-energy regime, perturbation theory can be applied.
At small energies, perturbation theory breaks down and an another approach is needed. Lattice QCD [6] can be used to solve the QCD numerically in the non-perturbative sector. In this way, the QCD phase diagram can be investigated for finite temperature and zero chemical potential[1]. The QCD phase diagram, which is shown in Fig.1.1, describes the different states of QCD matter and can be divided roughly into several regions [7, 8]. At low temperature and chemical potential, the quarks and gluons are bound to hadrons (hadronic phase). Increasing the temperature at fixed chemical potential, a crossover transition from confined to deconfined matter occurs and a state of weakly-coupled quarks and gluons, called quark-gluon plasma (QGP) appears. For high μ and small T there also could exist a color-superconducting phase [9]. In the region at low temperature and intermediate chemical potential, crystalline structures are suggested, which could be characterized by spatially dependent condensates.

The idea of an inhomogeneous ground state was already discussed by Overhauser in 1960 [10]. Inhomogeneous phases were also investigated in the solid-state physics for superconductors with a single plane wave [11] as well as with a sinusoidal modulation [12]. Though, lattice calculations fail to describe this region since the Monte Carlo sampling method does not work anymore due to the complex fermion determinant for finite chemical potential. This is known as the "fermion sign problem" [8]. To overcome this complication, there are different ways e.g. simulating pure imaginary chemical potential and finding the physical quantities by using the analytic continuation backwards to obtain real chemical potential, or using Taylor expansion in terms of μ/T. A less problematic approach is to formulate effective models which share important properties with the QCD e.g. Nambu–Jona-Lasinio (NJL) model [13, 14] or the quark-meson model [15, 16].
In this thesis we will work with the NJL model in mean-field approximation to study inhomogeneous phases. For the spatial modulation of the chiral condensate, we choose a Fourier expansion with a finite number of coefficients. The Fourier amplitudes can be obtained by looking at the extrema of the corresponding thermodynamic potential. This can be done with the numerical minimization of the thermodynamic potential. Another way is to derive the thermodynamic potential with respect to the Fourier coefficients. This results in a system of coupled integro-differential equations, called gap equations.

[1] The chemical potential is associated with baryon number conservation.

The aim of this work is to build up new solutions for higher coefficients from the gap equation system with fewer Fourier coefficients via fixed-point iterations instead of minimizing the corresponding thermodynamic potential.

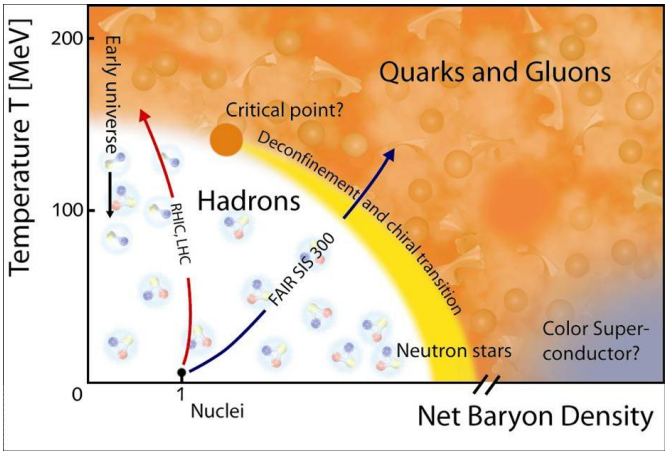

Figure 1.1: QCD phase diagram taken from [20].

Structure of the document

In chapter 2, we introduce the NJL model and derive the gap equations in the context of inhomogeneous phases. Before moving on with the gap system at inhomogeneous regions, the homogeneous case is briefly studied in chapter 3. In the fourth chapter, we will restrict ourselves to one-dimensional modulations to develop some simplifications for the numerical framework. This is used to present numerical results for the Fourier ansatz with higher coefficients in chapter 5 and compare them with the solitonic solution. At the end, we recapitulate all discussed results in chapter 6 and deliver insight into outstanding tasks.

2 Nambu–Jona-Lasinio model

The Nambu–Jona-Lasinio (NJL) model arose in 1961, before the QCD was introduced. The original idea behind this model was the description of the dynamical mass generation of the nucleons in analogy to the energy gap in the BCS-theory of superconductors [13, 14]. Later the nucleon fields were substituted by quark fields to describe non-pertubative effects of QCD with local quark-antiquark interaction terms. The advantage of the NJL model is that it is based on symmetries e.g. it has the same global symmetries as QCD including spontaneous symmetry breaking. Therefore, it is often used as a simple model to study chiral symmetry and their restoration in the medium. In contrast, the NJL model does not contain confinement and gluons, which means that hadrons in this model can decay into quarks (indicated by an imaginary part in the Bethe-Salpeter equation). Rather, the gluonic degrees of freedom are incorporated in the point-like quark-antiquark interaction. Another drawback of this model is the non-renormalizability caused by the local four-point interactions. Thereby an additional parameter has to be introduced to regularize the divergent integrals to finite values.

2.1 The NJL-Lagrangian

The NJL Lagrangian consists of a free part $\mathscr{L}_{\text{free}}$ and an interaction part $\mathscr{L}_{\text{int}}$

$$\mathscr{L}_{\text{NJL}} = \mathscr{L}_{\text{free}} + \mathscr{L}_{\text{int}} \tag{2.1}$$

given by

$$\mathscr{L}_{\text{free}} = \bar{\psi}\left(i\gamma^{\mu}\partial_{\mu} - m\right)\psi \tag{2.2}$$

$$\mathscr{L}_{\text{int}} = \sum_{N} g_N \left(\bar{\psi}\Gamma_N\psi\right)^2 \tag{2.3}$$

where ψ are the quark fields, γ^{μ} are the Dirac matrices, m is the current quark mass and Γ_N are the interaction channels with the associated coupling constants g_N. The quark fields are embedded in the time, position, Dirac, isospin and color space. In this work, we regard up and down quarks ($N_{\text{f}} = 2$) with three color charges ($N_{\text{c}} = 3$) as degenerated, so their masses are equal: $m := m_{\text{u}} = m_{\text{d}}$. In addition, only the scalar $\Gamma_S = \mathbb{1}$ and the pseudoscalar $\Gamma_P^a = \bar{\psi} i\gamma_5\tau^a\psi$ channel are considered:

$$\mathscr{L}_{\text{NJL}} = \bar{\psi}\left(i\gamma^{\mu}\partial_{\mu} - m\right)\psi + g_{\text{s}}\left[\left(\bar{\psi}\psi\right)^2 + \left(\bar{\psi}i\gamma_5\vec{\tau}\psi\right)^2\right] \tag{2.4}$$

Here, τ^a, $a \in \{1,2,3\}$ are the Pauli matrices in isospin space. The interaction terms $\bar{\psi}\psi$ and $\bar{\psi}i\gamma_5\tau^a\psi$ can be converted into each other by axial transformations. To preserve the chiral symmetry of $\mathscr{L}_{\text{NJL}}$ the coupling constants of the scalar and pseudoscalar channel have to be the same.
The NJL Lagrangian (2.4) shares the same global symmetries with QCD. The invariance of the Lagrangian according to these symmetries leads to conservation of physical quantities as a consequence of the Noether theorem. In the following, we want to discuss some of the shared symmetries.
The invariance of $\mathscr{L}_{\text{NJL}}$ under global phase transformation $U_{\text{V}}(1)$

$$\psi \to \exp(-i\alpha)\psi \quad \text{and} \quad \bar{\psi} \to \exp(i\alpha)\bar{\psi} \quad \text{with} \quad \alpha \in \mathbb{R} \tag{2.5}$$

gives rise to the conservation of baryon number.
In the isospin limit $m_u = m_d$, the NJL Lagrangian becomes invariant under rotations in isospin space ($SU_V(2)$ transformation)

$$\psi \to \exp\left(-\frac{i}{2}\vec{\tau}\vec{\omega}\right)\psi \quad \text{and} \quad \bar{\psi} \to \bar{\psi}\exp\left(\frac{i}{2}\vec{\tau}\vec{\omega}\right) \quad \text{with} \quad \vec{\omega} \in \mathbb{R}^3 \tag{2.6}$$

which results in conservation of isospin. This symmetry is not exactly fulfilled in the QCD, since the masses of up and down quarks differ slightly from each other.
The third symmetry is the axial transformation $SU_A(2)$, which changes the quark fields as follows:

$$\psi \to \exp\left(-\frac{i}{2}\gamma_5\vec{\tau}\vec{\theta}\right)\psi \quad \text{and} \quad \bar{\psi} \to \bar{\psi}\exp\left(-\frac{i}{2}\gamma_5\vec{\tau}\vec{\theta}\right) \quad \text{with} \quad \vec{\theta} \in \mathbb{R}^3 \tag{2.7}$$

The NJL Lagrangian is only invariant under this transformation if the chiral limit $m = m_u = m_d = 0$ is considered. Thus, $SU_A(2)$ is explicitly broken by the non-vanishing current quark mass. Due to interaction terms in the Lagrangian, an effective mass (constituent quark mass) can be generated and leads to spontaneous symmetry breaking in the vacuum. The quark condensate $\langle\bar{\psi}\psi\rangle$, which is connected to the effective mass (see equation (2.30)), can be considered as the order parameter of symmetry breaking. The combination of the vector and axial symmetry is called the chiral symmetry $SU_V(2) \otimes SU_A(2)$ which is approximately fulfilled.

2.2 Thermodynamic potential

The thermodynamic potential is an important physical quantity because it contains information about the thermodynamic system. In statistical physics, one usually works with three kinds of ensembles in the thermodynamic equilibrium.
In the micro canonical ensemble, the total energy E, the number of particles N and the volume V are fixed, so it describes an isolated system.
The canonical ensemble describes a closed system where the particles can exchange energy with a heat bath, but the particle number, the volume and the temperature T are fixed.
The grand canonical ensemble characterizes an open system, so that the energy and the particles can be exchanged with a heat reservoir, but the temperature and the chemical potential μ are specified.
Since in a quantum field theory (QFT), particles can be created or annihilated, the grand canonical ensemble is used to describe the thermodynamic properties of a relativistic quantum system. The grand canonical thermodynamic potential per volume [2] is defined by

$$\Omega(T,\mu) = -\frac{T}{V}\ln\mathscr{Z}(T,\mu). \tag{2.8}$$

With the grand canonical partition function $\mathscr{Z}(T,\mu)$ one can derive other important average quantities like pressure P, net particle number N or the entropy S

$$P = \left.\frac{\partial(T\ln\mathscr{Z})}{\partial V}\right|_{T,\mu}, N = \left.\frac{\partial(T\ln\mathscr{Z})}{\partial\mu}\right|_{T,V}, S = \left.\frac{\partial(T\ln\mathscr{Z})}{\partial T}\right|_{V,\mu} \tag{2.9}$$

as well as the energy

$$E = -PV + TS + \mu N. \tag{2.10}$$

The partition function is given by

$$\mathscr{Z}(T,\mu) = \mathbf{Tr}\exp\left[-\frac{1}{T}\int \mathrm{d}^3\vec{x}\left(\mathscr{H} - \mu\bar{\psi}\gamma^0\psi\right)\right] \tag{2.11}$$

where the functional trace is taken over all states of the system. The Hamiltonian density $\mathscr{H}$ can be obtained by the Legendre transformation of the Lagrangian. The spatial integration of the baryon number

[2] For simplicity we will refer it as 'thermodynamic potential'.

density $\mu\bar{\psi}\gamma^0\psi$ corresponds to the baryon number conservation. In terms of the path integral formalism, the partition function reads

$$\mathcal{Z}(T,\mu) = \int \mathcal{D}\bar{\psi}\mathcal{D}\psi \ \exp\left(\int_0^{1/T} \mathrm{d}\tau \int \mathrm{d}^3\vec{x} \ \left(\mathcal{L}_{\mathrm{NJL}} + \mu\bar{\psi}\gamma^0\psi\right)\right) \tag{2.12}$$

with the imaginary time $\tau = it$ and the Grassmann variables $\bar{\psi}, \psi$. To integrate out the expression above, the mean-field approximation on the NJL-Lagrangian will be applied. The interaction terms are expanded around their expectation values i.e. replaced by the scalar and the pseudoscalar condensate $\langle\bar{\psi}\psi\rangle$ and $\langle\bar{\psi}i\gamma^5\tau^a\psi\rangle$ plus small fluctuations:

$$\bar{\psi}\psi = \phi_S + \delta\phi_S \tag{2.13}$$
$$\bar{\psi}i\gamma^5\tau^a\psi = \phi_P^a + \delta\phi_P^a \tag{2.14}$$
$$\Longrightarrow \tag{2.15}$$
$$\left(\bar{\psi}\psi\right)^2 = (\phi_S + \delta\phi_S)^2 = \phi_S^2 + 2\phi_S\delta\phi_S + (\delta\phi_S)^2 = -\phi_S^2 + 2\phi_S\bar{\psi}\psi + (\delta\phi_S)^2 \tag{2.16}$$
$$\left(\bar{\psi}i\gamma^5\vec{\tau}\psi\right)^2 = \sum_{a=1}^{3}\left(\phi_P^a + \delta\phi_P^a\right)^2 = \left(\vec{\phi}_P\right)^2 + 2\vec{\phi}_P\delta\vec{\phi}_P + \left(\delta\vec{\phi}_P\right)^2 = -\left(\vec{\phi}_P\right)^2 + 2\bar{\psi}i\gamma^5\vec{\tau}\vec{\phi}_P\psi + \left(\delta\vec{\phi}_P\right)^2 \tag{2.17}$$

with

$$\phi_S = \langle\bar{\psi}\psi\rangle \tag{2.18}$$
$$\phi_P^a = \langle\bar{\psi}i\gamma^5\tau^a\psi\rangle\,. \tag{2.19}$$

Inserting this into the NJL-Lagrangian and neglecting quadratic fluctuation terms, yields the mean-field Lagrangian

$$\mathcal{L}_{\mathrm{MF}} + \mu\bar{\psi}\gamma^0\psi = \bar{\psi}S^{-1}\psi - \mathcal{V} \tag{2.20}$$

with the inverse propagator

$$S^{-1}(x) = i\gamma^\mu\partial_\mu - m + \gamma^0\mu + 2g_s\left(\phi_S(x) + i\gamma^5\vec{\tau}\vec{\phi}_P(x)\right) \tag{2.21}$$

and the condensate part

$$\mathcal{V}(x) = g_s\left(\phi_S^2(x) + \vec{\phi}_P^2(x)\right). \tag{2.22}$$

From now on, the path integration

$$\mathcal{Z}_{\mathrm{MF}}(T,\mu) = \int \mathcal{D}\bar{\psi}\mathcal{D}\psi \ \exp\left(\int_0^{1/T} \mathrm{d}\tau \int \mathrm{d}^3\vec{x} \ \left(\bar{\psi}(x)\, S^{-1}(x)\, \psi(x) - \mathcal{V}(x)\right)\right) \tag{2.23}$$

can be performed due to the bilinearity of the Grassmann fields. Before doing this, few simplifications have to be done for further calculations. Firstly, a static medium is assumed. This means, that the condensates will only depend on spatial coordinates. So, the inverse propagator can be divided into a time- and space-dependent part

$$S^{-1}(x) = \gamma^0\left[-\partial_\tau - H(\vec{x}) + \mu\right] \tag{2.24}$$

with the effective Hamiltonian

$$H(\vec{x}) := \gamma^0 \left[-i\vec{\gamma}\vec{\nabla} + m - 2g_s \left(\phi_S(\vec{x}) + i\gamma^5 \vec{\tau}\vec{\phi}_P(\vec{x}) \right) \right]. \tag{2.25}$$

Secondly, we vary the pseudo scalar condensate only in the 3-direction in flavor space

$$\phi_P^a(\vec{x}) = \phi_P(\vec{x})\ \delta_{a,3} \tag{2.26}$$

so that the effective Hamiltonian becomes a direct product in the isospin space

$$H(\vec{x}) = H^+(\vec{x}) \otimes H^-(\vec{x}) \tag{2.27}$$

with

$$H^\pm(\vec{x}) = \gamma^0 \left[-i\vec{\gamma}\vec{\nabla} + m - 2g_s \left(\phi_S(\vec{x}) \pm i\gamma^5 \phi_P(\vec{x}) \right) \right] \tag{2.28}$$

or in the Weyl representation

$$H^\pm(\vec{x}) = \begin{pmatrix} i\vec{\sigma}\vec{\nabla} & M^\pm(\vec{x}) \\ M^\mp(\vec{x}) & -i\vec{\sigma}\vec{\nabla} \end{pmatrix}. \tag{2.29}$$

Here, $\vec{\sigma}$ is the Pauli vector in spin space and $M^\pm(\vec{x})$ are the mass functions which we define by:

$$M^\pm(\vec{x}) = m - 2g_s \left[\phi_S(\vec{x}) \pm i\phi_P(\vec{x}) \right] \tag{2.30}$$

$$M^+(\vec{x}) = M(\vec{x}) \tag{2.31}$$

$$M^-(\vec{x}) = M^*(\vec{x}) \tag{2.32}$$

Due to isospin invariance, both Hamiltonians H^+ and H^- have the same eigenvalues. This will later result in a degeneracy factor $N_\mathrm{f} = 2$. In the following, we assume that the mass functions are periodic in space, i.e.

$$M^\pm(\vec{x}) = M^\pm(\vec{x} + \vec{n}_i),\ i \in \{1, 2, 3\} \tag{2.33}$$

where $\vec{n}_i$ are the basis vectors of the unit cell. From that, it follows the Fourier decomposition of the mass functions

$$M^\pm(\vec{x}) = \sum_{\vec{q}_k} M^\pm_{\vec{q}_k} e^{\pm i\vec{q}_k\vec{x}}. \tag{2.34}$$

The discrete momenta $\vec{q}_k$ form the reciprocal lattice (R.L.) and satisfy the condition $\vec{q}_k\vec{n}_i = 2\pi n_{ik}$ with $n_{ik} \in \mathbb{Z}$, which can be obtained by inserting the Fourier decomposition (2.34) into equation (2.33). At this point, we will work in momentum space and consider the volume V composed of multiples $N \in \mathbb{N}$ of the unit cell. Thus, the momenta obey the following condition

$$\vec{p}_m \cdot \vec{n}_i = 2\pi \frac{N_{mi}}{N} \text{ with } N_{mi} \in \mathbb{Z}. \tag{2.35}$$

Hence, the quark fields can be expanded in Fourier series:

$$\psi(x) = \frac{1}{\sqrt{V}} \sum_{p_\mathrm{n}} \psi_{p_\mathrm{n}} e^{-ip_\mathrm{n}x} = \frac{1}{\sqrt{V}} \sum_{\omega_\mathrm{n}} \sum_{\vec{p}_\mathrm{n}} \psi_{p_\mathrm{n}} e^{-i(\omega_\mathrm{n}\tau - \vec{p}_\mathrm{n}\vec{x})} \tag{2.36}$$

$$\bar{\psi}(x) = \frac{1}{\sqrt{V}} \sum_{p_\mathrm{n}} \bar{\psi}_{p_\mathrm{n}} e^{ip_\mathrm{n}x} = \frac{1}{\sqrt{V}} \sum_{\omega_\mathrm{n}} \sum_{\vec{p}_\mathrm{n}} \bar{\psi}_{p_\mathrm{n}} e^{i(\omega_\mathrm{n}\tau - \vec{p}_\mathrm{n}\vec{x})} \tag{2.37}$$

The fermion fields are anti periodic in the imaginary time component, i.e. $\psi(0,\vec{x}) = -\psi(1/T,\vec{x})$. This implies that the Matsubara frequencies ω_n take the form $\omega_n = (2n+1)\pi T$. With the transformed fields (2.36), (2.37) and the periodic mass function ansatz (2.34), the path integral (2.12) can now be evaluated

$$\mathscr{Z}_{\mathrm{MF}}(T,\mu) = \det\left(\frac{S^{-1}_{\vec{p}}}{T}\right)\cdot\exp\left(-\int_0^{1/T}\mathrm{d}\tau\int\mathrm{d}^3\vec{x}\;\mathscr{V}(x)\right) \tag{2.38}$$

where the inverse propagator in momentum space (see App. C.2) is given by

$$S^{-1}_{p_m,p_n} = \delta_{\omega_\mathrm{n},\omega_\mathrm{m}}\gamma^0\left[i\omega_\mathrm{n}\delta_{\vec{p}_\mathrm{n},\vec{p}_\mathrm{m}} - \underbrace{\left(H^+_{\vec{p}_\mathrm{m},\vec{p}_\mathrm{n}}\otimes H^-_{\vec{p}_\mathrm{m},\vec{p}_\mathrm{n}}\right)}_{=H_{\vec{p}_\mathrm{m},\vec{p}_\mathrm{n}}} + \mu\delta_{\vec{p}_\mathrm{n},\vec{p}_\mathrm{m}}\right] \tag{2.39}$$

with the Hamiltonian $H_{\vec{p}_\mathrm{m},\vec{p}_\mathrm{n}} = H^+_{\vec{p}_\mathrm{m},\vec{p}_\mathrm{n}}\otimes H^-_{\vec{p}_\mathrm{m},\vec{p}_\mathrm{n}}$ (see App. C.1) in momentum space

$$H^\pm_{\vec{p}_\mathrm{m},\vec{p}_\mathrm{n}} = \gamma^0\vec{\gamma}\vec{p}_\mathrm{n}\delta_{\vec{p}_\mathrm{n},\vec{p}_\mathrm{m}} + \sum_{\vec{q}_\mathrm{k}} M^\pm_{\vec{q}_\mathrm{k}}\delta_{\vec{p}_\mathrm{m},\vec{p}_\mathrm{n}\pm\vec{q}_\mathrm{k}}\gamma^0 P_+ + \sum_{\vec{q}_\mathrm{k}} M^\mp_{\vec{q}_\mathrm{k}}\delta_{\vec{p}_\mathrm{m},\vec{p}_\mathrm{n}\mp\vec{q}_\mathrm{k}}\gamma^0 P_- \tag{2.40}$$

$$= \begin{pmatrix} -\vec{\sigma}\vec{p}_\mathrm{n}\delta_{\vec{p}_\mathrm{n},\vec{p}_\mathrm{m}} & \sum_{\vec{q}_\mathrm{k}} M^\pm_{\vec{q}_\mathrm{k}}\delta_{\vec{p}_\mathrm{m},\vec{p}_\mathrm{n}\pm\vec{q}_\mathrm{k}} \\ \sum_{\vec{q}_\mathrm{k}} M^\mp_{\vec{q}_\mathrm{k}}\delta_{\vec{p}_\mathrm{m},\vec{p}_\mathrm{n}\mp\vec{q}_\mathrm{k}} & \vec{\sigma}\vec{p}_\mathrm{n}\delta_{\vec{p}_\mathrm{n},\vec{p}_\mathrm{m}} \end{pmatrix} \tag{2.41}$$

and the chirality projectors in Dirac space

$$P_\pm = \frac{1}{2}\left(1\pm\gamma^5\right). \tag{2.42}$$

The Hamiltonian is in general not diagonal in infinite-dimensional momentum space, since the in- and outgoing quarks can exchange momenta by scattering off the non-uniform condensate. In the homogeneous case $M(\vec{x}) = const.$, the Hamiltonian becomes a diagonal matrix in momentum space, so that the in- and outgoing quarks carry the same momenta ($\vec{q}_k = 0$).
Inserting the partition function (2.38) into equation (2.8) leads to the thermodynamic potential, which separates in a kinetic Ω_{kin} and a condensate part Ω_{cond}:

$$\Omega_{\mathrm{MF}}(T,\mu) = -\frac{T}{V}\ln\mathscr{Z}_{\mathrm{MF}}(T,\mu) \tag{2.43}$$

$$= \Omega_{\mathrm{kin}} + \Omega_{\mathrm{cond}} \tag{2.44}$$

where

$$\Omega_{\mathrm{kin}} = -\frac{T}{V}\ln\det\left(\frac{S^{-1}_{\vec{p}}}{T}\right) = -\frac{T}{V}\mathrm{Tr}\ln\left(\frac{S^{-1}_{\vec{p}}}{T}\right) \tag{2.45}$$

$$\Omega_{\mathrm{cond}} = \frac{1}{V}\int\mathrm{d}^3\vec{x}\;\frac{|M(\vec{x})-m|^2}{4g_s} \overset{(2.34)}{=} \sum_{\vec{q}_k}\frac{\left|M_{\vec{q}_k} - m\delta_{\vec{q}_k,0}\right|^2}{4g_s}. \tag{2.46}$$

The trace in the kinetic part runs over the color, flavor, Dirac, frequencies and momentum space. Since the inverse propagator $S^{-1}_{p_m,p_n}$ is diagonal in the Matsubara frequencies[3] and in color and flavor space, the trace results in a sum over the Matsubara frequencies times the trivial contribution $N_\mathrm{c}N_\mathrm{f}$:

$$\Omega_{\mathrm{kin}} = -\frac{T}{V}\mathrm{Tr}\ln\left(\frac{S^{-1}_{\vec{p}}}{T}\right) = -\frac{T}{V}N_\mathrm{f}N_\mathrm{c}\sum_n\mathrm{tr}_{\mathrm{Dirac},\vec{p}}\left[\ln\left(\frac{1}{T}\left(i\omega_\mathrm{n} - H^+_{\vec{p}} + \mu\right)\right)\right] \tag{2.47}$$

$$= -\frac{T}{V}N_\mathrm{f}N_\mathrm{c}\sum_{E_\lambda}\sum_n\ln\left(\frac{1}{T}\left(i\omega_\mathrm{n} - E_\lambda + \mu\right)\right) \tag{2.48}$$

[3] It is a consequence of the assumption of static condensates which satisfy energy conservation.

In the last step, we assume that the hermitian Hamiltonian H^+ is already diagonalized and has the eigenvalues E_λ in Dirac and momentum space[4]. Applying the Matsubara formalism [21] (see App. D), yields

$$\Omega_{\text{kin}}(T,\mu) = -\frac{T}{V} N_{\text{f}} N_{\text{c}} \sum_{E_\lambda} \ln\left[2\cosh\left(\frac{E_\lambda - \mu}{2T}\right)\right] \tag{2.49}$$

$$= -\frac{T}{V} N_{\text{f}} N_{\text{c}} \sum_{E_\lambda} \left[\frac{E_\lambda - \mu}{2T} + \ln\left(1 + \exp\left(-\frac{E_\lambda - \mu}{T}\right)\right)\right]. \tag{2.50}$$

Due to the large size of the Hamiltonian matrix, the numerical diagonalization is very demanding. However, we can use the Bloch theorem [22] to simplify the matrix structure. It says that the eigenstates, which belong to different vectors of the first Brillouin zone (B.Z.), are orthogonal, i.e. by writing the in- and outgoing quark momenta as

$$\vec{p}_m = \vec{k}_m + \vec{q}_m \tag{2.51}$$

$$\vec{p}_n = \vec{k}_n + \vec{q}_n \tag{2.52}$$

for $\vec{k}_m, \vec{k}_n \in$ B.Z. and $\vec{q}_m, \vec{q}_n \in$ R.L., we can the use fact that the in- and outgoing momenta are only coupled by an element $\vec{q}_k$ of the reciprocal lattice. This can be seen from the Hamiltonian (2.41). Then, it follows from the momentum difference

$$\vec{p}_m - \vec{p}_n = \underbrace{\vec{k}_m - \vec{k}_n}_{\in \text{B.Z.}} + \underbrace{\vec{q}_m - \vec{q}_n}_{\in \text{R.L.}} \tag{2.53}$$

that the quark momenta are coupled if $\vec{k}_m = \vec{k}_n$ is valid. As a consequence, the Hamiltonian can be decomposed into a direct sum of Hamiltonian blocks in the first Brillouin zone

$$H^+ = \bigoplus_{\vec{k}_n \in \text{B.Z.}} H^+(\vec{k}_n) = \bigoplus_{\vec{k}_n \in \text{B.Z.}} P_{\vec{k}_n} H^+ \tag{2.54}$$

where we define the projector which projects out the blocks of the Hamiltonian H^+ [23]:

$$\left(P_{\vec{k}_n}\right)_{\vec{p}_m, \vec{p}_n} = \sum_{\vec{q}_m, \vec{q}_n \in \text{R.L.}} \delta_{\vec{p}_m - \vec{k}_n, \vec{q}_m} \delta_{\vec{p}_n - \vec{k}_n, \vec{q}_n} \tag{2.55}$$

Accordingly, the kinetic part of the thermodynamic potential can be written as

$$\Omega_{\text{kin}}(T,\mu) = -\frac{N_{\text{f}} N_{\text{c}}}{V} \sum_{\vec{k}_n \in \text{B.Z.}} \sum_{E_\lambda} \left[\frac{E_\lambda(\vec{k}_n) - \mu}{2} + T \ln\left(1 + \exp\left(-\frac{E_\lambda(\vec{k}_n) - \mu}{T}\right)\right)\right] \tag{2.56}$$

where $E_\lambda(\vec{k}_n)$ are now the eigenvalues of $H^+(\vec{k}_n)$. Performing the infinite volume limit

$$\frac{1}{V} \sum_{\vec{k}_n \in \text{B.Z.}} \to \int_{\text{B.Z.}} \frac{\mathrm{d}^3 \vec{k}}{(2\pi)^3} \tag{2.57}$$

yields

$$\Omega_{\text{kin}}(T,\mu) = -N_{\text{f}} N_{\text{c}} \int_{\text{B.Z.}} \frac{\mathrm{d}^3 \vec{k}}{(2\pi)^3} \sum_{E_\lambda} \left[\frac{E_\lambda(\vec{k}) - \mu}{2} + T \ln\left(1 + \exp\left(-\frac{E_\lambda(\vec{k}) - \mu}{T}\right)\right)\right]. \tag{2.58}$$

[4] Note: Since H^+ and H^- have the same eigenvalues, we chose here H^+.

If the eigenvalues spectrum consists of $\pm|E_\lambda|$ pairs , the above equation can be transformed into

$$\Omega_{\text{kin}}(T,\mu) = -N_{\text{f}}N_{\text{c}}\int_{\text{B.Z.}}\frac{\mathrm{d}^3\vec{k}}{(2\pi)^3}\sum_{E_\lambda>0}\left[\underbrace{E_\lambda(\vec{k})}_{=:f_{\text{vac}}(E_\lambda)} + \underbrace{T\sum_{s\in\{-1,1\}}\ln\left(1+\exp\left(-\frac{E_\lambda(\vec{k})-s\mu}{T}\right)\right)}_{=:f_{\text{med}}(E_\lambda,T,\mu)}\right]. \tag{2.59}$$

The vacuum contribution $f_{\text{vac}}(E_\lambda)$ is divergent and thus has to be regularized. This will be done in section 2.4. In contrast to, the medium contribution $f_{\text{med}}(E_\lambda,T,\mu)$ is finite due to the exponential functions and will not be regularized, since a regularization will lead to non-physical artifacts of the chemical potential [19].
Finally, the total thermodynamic potential in momentum space reads

$$\begin{aligned}\Omega_{\text{MF}}(T,\mu) = -N_{\text{f}}N_{\text{c}}\int_{\text{B.Z.}}\frac{\mathrm{d}^3\vec{k}}{(2\pi)^3}\sum_{E_\lambda}\left[\frac{E_\lambda(\vec{k})-\mu}{2} + T\ln\left(1+\exp\left(-\frac{E_\lambda(\vec{k})-\mu}{T}\right)\right)\right]\\ +\sum_{\vec{q}_k}\frac{\left|M_{\vec{q}_k}-m\delta_{\vec{q}_k,0}\right|^2}{4g_s}.\end{aligned} \tag{2.60}$$

2.3 Gap equations

The stationary solutions $M_{\vec{q}_k}$ can be obtained by minimizing the thermodynamic potential. Numerically, this can be done by minimizing the potential directly with a minimization algorithm e.g. [24] or by deriving the thermodynamic potential with respect to $M_{\vec{q}_k}$ or $M^*_{\vec{q}_k}$, and solving the corresponding system of coupled integro-differential equations (called gap equations). The first option was already used by Stefano Carignano [19]. Therefore, we will work with the second option and solve the gap equations by a fixed-point iteration. In case of several solutions $M_{\vec{q}_k}$, the ones which are the global minima of the thermodynamic potential will be taken.
The stationary condition

$$\frac{\partial\Omega_{\text{MF}}}{\partial M^*_{\vec{q}_k}} \stackrel{!}{=} 0 \tag{2.61}$$

yields the gap equations

$$M_{\vec{q}_k} - m\delta_{\vec{q}_k,0} = 2N_{\text{f}}N_{\text{c}}g_s\int_{\text{B.Z.}}\frac{\mathrm{d}^3\vec{k}}{(2\pi)^3}\sum_{E_\lambda}\left[\frac{\partial E_\lambda(\vec{k})}{\partial M^*_{\vec{q}_k}}\cdot\tanh\left(\frac{E_\lambda(\vec{k})-\mu}{2T}\right)\right]. \tag{2.62}$$

The above equations require to determine the derivative of the eigenvalues with respect to the Fourier coefficients. Currently, no analytic expressions for the eigenvalues, except for the homogeneous, solitonic and chiral density wave case in the chiral limit, exist. So, one has to prepare the gap equations for numerical calculations to get useful results. Here, we can exploit the hermiticity of the Hamiltonian, so that the eigenvalues can be written as

$$E_\lambda(\vec{k}) = \omega^\dagger_\lambda(\vec{k})\,H^+(\vec{k})\,\omega_\lambda(\vec{k}) \tag{2.63}$$

where $\omega_\lambda(\vec{k})$ are the normalized eigenvectors of $H^+(\vec{k})$. The derivative of the eigenvalues can be further simplified by using the orthonormalization relation of the eigenvectors (see Hellmann-Feynman theorem [25, 26])

$$\frac{\partial E_\lambda(\vec{k})}{\partial M^*_{\vec{q}_k}} = E_\lambda(\vec{k})\left(\frac{\partial \omega^\dagger_\lambda(\vec{k})}{\partial M^*_{\vec{q}_k}}\omega_\lambda(\vec{k}) + \omega^\dagger_\lambda(\vec{k})\frac{\partial \omega_\lambda(\vec{k})}{\partial M^*_{\vec{q}_k}}\right) + \omega^\dagger_\lambda(\vec{k})\frac{\partial H^+(\vec{k})}{\partial M^*_{\vec{q}_k}}\omega_\lambda(\vec{k}) \tag{2.64}$$

$$= E_\lambda(\vec{k})\underbrace{\frac{\partial\left(\omega^\dagger_\lambda(\vec{k})\,\omega_\lambda(\vec{k})\right)}{\partial M^*_{\vec{q}_k}}}_{=0} + \omega^\dagger_\lambda(\vec{k})\,\frac{\partial H^+(\vec{k})}{\partial M^*_{\vec{q}_k}}\,\omega_\lambda(\vec{k}) \tag{2.65}$$

$$= \omega^\dagger_\lambda(\vec{k})\,\frac{\partial H^+(\vec{k})}{\partial M^*_{\vec{q}_k}}\,\omega_\lambda(\vec{k}) \tag{2.66}$$

$$\overset{(2.41)}{=} \sum_{\vec{p}_m,\vec{p}_n}\left(\omega_\lambda(\vec{k})\right)^\dagger_{\vec{p}_m}\delta_{\vec{p}_m,\vec{p}_n-\vec{q}_k}\,\gamma^0 P_-\,\left(\omega_\lambda(\vec{k})\right)_{\vec{p}_n} \tag{2.67}$$

$$= \sum_{\vec{p}_m}\left(\omega^{\mathrm{R}}_\lambda(\vec{k})\right)^\dagger_{\vec{p}_m}\,\left(\omega^{\mathrm{L}}_\lambda(\vec{k})\right)_{\vec{p}_m+\vec{q}_k} \tag{2.68}$$

with the right- and left-handed eigenvectors $\omega^{\mathrm{R}}_\lambda(\vec{k})$ and $\omega^{\mathrm{L}}_\lambda(\vec{k})$ in chiral basis:

$$\omega^{\mathrm{L/R}}_\lambda(\vec{k}) = P_\pm\omega_\lambda(\vec{k}) \tag{2.69}$$

So, we end up with the following gap equations

$$M_{\vec{q}_k} - m\delta_{\vec{q}_k,0} = 2N_{\mathrm{f}}N_{\mathrm{c}}g_s\int_{\mathrm{B.Z.}}\frac{\mathrm{d}^3\vec{k}}{(2\pi)^3}\sum_{E_\lambda}\left[\left(\sum_{\vec{p}_m}\left(\omega^{\mathrm{R}}_\lambda(\vec{k})\right)^\dagger_{\vec{p}_m}\,\left(\omega^{\mathrm{L}}_\lambda(\vec{k})\right)_{\vec{p}_m+\vec{q}_k}\right)\cdot\tanh\left(\frac{E_\lambda(\vec{k})-\mu}{2T}\right)\right] \tag{2.70}$$

or in terms of eigenvalues pairs $\pm|E_\lambda|$

$$M_{\vec{q}_k} - m\delta_{\vec{q}_k,0} = 4N_{\mathrm{f}}N_{\mathrm{c}}g_s\int_{\mathrm{B.Z.}}\frac{\mathrm{d}^3\vec{k}}{(2\pi)^3}\sum_{E_\lambda>0}\left[\left(\sum_{\vec{p}_m}\left(\omega^{\mathrm{R}}_\lambda(\vec{k})\right)^\dagger_{\vec{p}_m}\,\left(\omega^{\mathrm{L}}_\lambda(\vec{k})\right)_{\vec{p}_m+\vec{q}_k}\right)\times\right.$$
$$\left.\times\left(1-n_{\mathrm{F}}(E_\lambda(\vec{k})-\mu)-n_{\mathrm{F}}(E_\lambda(\vec{k})+\mu)\right)\right] \tag{2.71}$$

with the Fermi function $n_{\mathrm{F}}(z) = [1+\exp(z/T)]^{-1}$. These equations are divergent and we will apply in the next section a suitable regularization scheme to the gap equations and the thermodynamic potential.

2.4 Regularization

The NJL model is non-renormalizable due to four-point interaction in the Lagrangian. So, the emerging divergences in the integrals need to be regularized. In Subsection 2.2 we have seen that the kinetic part of the thermodynamic potential splits into a divergent vacuum and a convergent medium part:

$$\Omega_{\mathrm{kin}}(T,\mu) = -N_{\mathrm{f}}N_{\mathrm{c}}\int_{\mathrm{B.Z.}}\frac{\mathrm{d}^3\vec{k}}{(2\pi)^3}\sum_{E_\lambda>0}\left[f_{\mathrm{vac}}(E_\lambda) + f_{\mathrm{med}}(E_\lambda,T,\mu)\right] \tag{2.72}$$

The regularization of the full integrand will produce non-physical artefacts of the chemical potential, so we will only apply a regularization scheme to the divergent part $f_{\mathrm{vac}}(E_\lambda)$. Since we deal with inhomogeneous phases, not all regularization schemes are suitable for our purpose. For example, a widely

used regularization scheme due to its simplicity is the three-momentum cutoff procedure. It limits the momentum integration boundary to a sharp cutoff $|\vec{k}| < \Lambda$ and thus, it is no more Lorentz-invariant. For inhomogeneous phases it has another drawback. The restriction to a certain momentum scale will restrict the coupled momenta of the quark condensate. Therefore we will not use this scheme in our thesis.
One possible choice is the Pauli-Villars regularization [27], which uses additional mass counter terms in the integrands to render the momentum integral finite. The added terms should have the same asymptotic behavior in the high momentum regime and their number depends on the degree of divergence. This scheme has the advantage that it is Lorentz- and gauge-invariant. Instead of mass terms we will add energy terms to the divergent part of the kinetic part of the thermodynamic potential

$$\Omega_{\text{kin}}(T,\mu) = -N_{\text{f}}N_{\text{c}}\int_{\text{B.Z.}}\frac{\mathrm{d}^3\vec{k}}{(2\pi)^3}\sum_{E_\lambda>0}\left[\sum_{j=0}^{3}c_j\cdot f_{\text{vac}}\left(\sqrt{\left(E_\lambda(\vec{k})\right)^2+j\Lambda^2}\right)+f_{\text{med}}\left(E_\lambda(\vec{k}),T,\mu\right)\right] \tag{2.73}$$

to get a finite value. The Pauli-Villars coefficients c_j of this energetic version of the Pauli-Villars regularization[5] have to be chosen that the counter parts obliterate each other for large energies. To render the thermodynamic potential finite, three counter terms are necessary:

$$c_0 = 1,\ c_1 = -3,\ c_2 = 3,\ c_3 = -1 \tag{2.74}$$

Respectively, the gap equations read

$$M_{\vec{q}_k} - m\delta_{\vec{q}_k,0} = 4N_{\text{f}}N_{\text{c}}g_s\int_{\text{B.Z.}}\frac{\mathrm{d}^3\vec{k}}{(2\pi)^3}\sum_{E_\lambda>0}\left[\frac{\partial E_\lambda(\vec{k})}{\partial M^*_{\vec{q}_k}}\left(\sum_{j=0}^{3}\frac{c_j\cdot E_\lambda(\vec{k})}{\sqrt{\left(E_\lambda(\vec{k})\right)^2+j\Lambda^2}}-\sum_{s\in\{-1,1\}}n_{\text{F}}(E_\lambda(\vec{k})-s\mu)\right)\right]. \tag{2.75}$$

In the chiral limit ($m = 0$), the cutoff Λ and the coupling constant g_s are fixed to the constituent quark mass $M_{\text{vac}} = 300$ MeV and the pion decay constant $f_\pi = 88$ MeV in vacuum (see table 2.1) by the equations

$$M_{\text{vac}} = m + 4g_sN_cN_fM_{\text{vac}}I_1^{\text{vac}}(M_{\text{vac}}) \tag{2.76}$$

$$f_\pi^2 = -\frac{N_cM_{\text{vac}}^2}{(2\pi)^2}\sum_{j=0}^{3}c_j\cdot\ln\left(\frac{M_{\text{vac}}^2+j\Lambda^2}{M_{\text{vac}}^2}\right) \tag{2.77}$$

with the analytically calculated integral

$$I_1^{\text{vac}}(M) = \frac{1}{(2\pi)^2}\sum_{j=0}^{3}\frac{c_j}{2}\cdot\left(M^2+j\Lambda^2\right)\cdot\ln\left(M^2+j\Lambda^2\right). \tag{2.78}$$

The first equation (2.76) is the homogeneous gap equation (see chapter 3). The second one (2.77) is taken from [28]. In the homogeneous case, the energetic version of the Pauli-Villars regularization corresponds to the standard form of the Pauli-Villars regularization by substituting the vacuum mass M_{vac} with $\sqrt{M_{\text{vac}}^2+j\Lambda^2}$. If not otherwise stated, we will use the parameters shown in Table 2.1 and treat the current quark mass m as a free parameter.

[5] This energetic version was obtained by a proper-time regularization of the functional logarithm in the thermodynamic potential [17].

Λ [MeV]	$g_s\Lambda^2$
757.048	6.002

Table 2.1: Parameter choice: The cutoff Λ and the coupling constant g_s are fitted to the constituent quark $M_{\text{vac}} = 300$ MeV and pion decay constant $f_\pi = 88$ MeV [29] at $T = 0$ and $\mu = 0$ in the chiral limit ($m = 0$).

3 Homogeneous case

3.1 Gap equation and thermodynamic potential

Before moving on with inhomogeneous phases, we want to discuss briefly some features of the homogeneous case. In the context of inhomogeneous phases, it will be clear that the homogeneous solutions will be important in our numerical framework.
In the homogeneous case, the chiral condensate is spatially constant. Accordingly, the momenta of the quarks do not couple and the full Hamiltonian consists of block diagonal matrices of the form:

$$H_{\vec{p}_\mathrm{m},\vec{p}_\mathrm{n}} = \begin{pmatrix} -\vec{\sigma}\vec{p}_\mathrm{n}\delta_{\vec{p}_\mathrm{n},\vec{p}_\mathrm{m}} & M_0\delta_{\vec{p}_\mathrm{m},\vec{p}_\mathrm{n}} \\ M_0\delta_{\vec{p}_\mathrm{m},\vec{p}_\mathrm{n}} & \vec{\sigma}\vec{p}_\mathrm{n}\delta_{\vec{p}_\mathrm{n},\vec{p}_\mathrm{m}} \end{pmatrix} \tag{3.1}$$

The eigenvalues of each block are given by $E_{\vec{k}} = \pm\sqrt{\vec{k}^2 + M_0^2}$ with $\vec{k} = \vec{p}_\mathrm{n}$. In this case, the integration over the Brillouin zone times the sum of the eigenvalues of each block in the thermodynamic potential, becomes an integral over the whole momentum space

$$\Omega_\mathrm{Hom} = -2N_\mathrm{c}N_\mathrm{f}\int \frac{\mathrm{d}^3\vec{k}}{(2\pi)^3}\left[\sum_{j=0}^{3} c_j\sqrt{E_{\vec{k}}^2 + j\Lambda^2} + T\ln\left(1+e^{-(E_{\vec{k}}-\mu)/T}\right) + T\ln\left(1+e^{-(E_{\vec{k}}+\mu)/T}\right)\right] + \frac{(M_0-m)^2}{4g_\mathrm{s}} \tag{3.2}$$

where the Pauli-Villars regularization $E_{\vec{k}} \to \sum_{j=0}^{3} c_j\sqrt{E_{\vec{k}}^2 + j\Lambda^2} = \sum_{j=0}^{3} c_j\sqrt{\vec{k}^2 + M_0^2 + j\Lambda^2}$ in the divergent part was applied. The factor 2 comes from the degeneracy of each eigenvalue. For the first term in the integral, one gets the analytical result:

$$J_1^\mathrm{vac}(M_0) = \int \frac{\mathrm{d}^3\vec{k}}{(2\pi)^3}\sum_{j=0}^{3} c_j\cdot\sqrt{\vec{k}^2 + M_0^2 + j\Lambda^2} = \frac{1}{(4\pi)^2}\sum_{j=0}^{3}\frac{c_j}{2}\cdot\left(M_0^2+j\Lambda^2\right)^2\cdot\ln\left(M_0^2+j\Lambda^2\right) \tag{3.3}$$

The medium part (second term)

$$J_1^\mathrm{med}(M_0,T,\mu) = \int \frac{\mathrm{d}^3\vec{k}}{(2\pi)^3}\left[T\ln\left(1+e^{-(E_{\vec{k}}-\mu)/T}\right) + T\ln\left(1+e^{-(E_{\vec{k}}+\mu)/T}\right)\right] \tag{3.4}$$

has to be integrated numerically. Overall, the thermodynamic potential can be written as:

$$\Omega_\mathrm{hom} = -2N_\mathrm{c}N_\mathrm{f}\left(J_1^\mathrm{vac}(M_0) + J_1^\mathrm{med}(M_0,T,\mu)\right) + \frac{(M_0-m)^2}{4g_\mathrm{s}} \tag{3.5}$$

Analogously, the gap equation reads

$$M_0 = m + 4M_0 g_\mathrm{s}N_\mathrm{c}N_\mathrm{f}\int \frac{\mathrm{d}^3\vec{k}}{(2\pi)^3}\left[\sum_{j=0}^{3}\frac{c_j}{\sqrt{E_{\vec{k}}^2+j\Lambda^2}} - \frac{1}{E_{\vec{k}}}\left(n_\mathrm{F}(E_{\vec{k}}-\mu) + n_\mathrm{F}(E_{\vec{k}}+\mu)\right)\right]. \tag{3.6}$$

Again, the first (vacuum) term in the integral can be integrated analytically and has the solution:

$$I_1^\mathrm{vac}(M_0) = \int \frac{\mathrm{d}^3\vec{k}}{(2\pi)^3}\sum_{j=0}^{3}\frac{c_j}{\sqrt{E_{\vec{k}}^2+j\Lambda^2}} = \frac{1}{(2\pi)^2}\sum_{j=0}^{3}\frac{c_j}{2}\left(M_0^2+j\Lambda^2\right)\ln\left(M_0^2+j\Lambda^2\right) \tag{3.7}$$

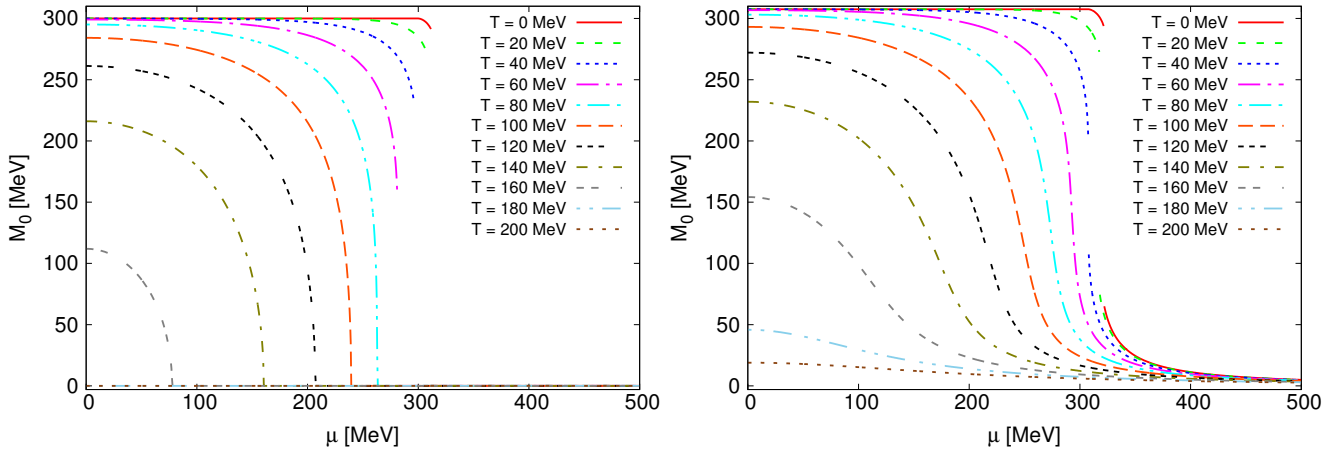

Figure 3.1: The effective mass M_0 was plotted against the chemical potential μ for different temperatures T in the chiral limit (left figure) and with finite bare quark mass $m = 5$ MeV (right figure).

The second (medium) term

$$I_1^{\text{med}}(M_0, T, \mu) = -\int \frac{\mathrm{d}^3\vec{k}}{(2\pi)^3} \frac{1}{E_{\vec{k}}} \left(n_{\text{F}}(E_{\vec{k}} - \mu) + n_{\text{F}}(E_{\vec{k}} + \mu) \right) \tag{3.8}$$

will be integrated numerically. With the above expressions, the gap equation can be written in a compact form:

$$M_0 = m + 4M_0 g_{\text{s}} N_{\text{c}} N_{\text{f}} \left(I_1^{\text{vac}}(M_0) + I_1^{\text{med}}(M_0, T, \mu) \right) \tag{3.9}$$

Both numerical integrations were performed with the `QAGI` algorithm from GSL [30], which uses a Gauss-Kronrod 15-point integration rule on infinite intervals.
The effective mass M_0 can be considered as an order parameter. The classification of the phase transitions can besides the Ehrenfest classification also be carried out by the order parameter. If the order parameter is discontinuous/continuous and not differentiable at the transition, then the transition is called first/second order transition. Otherwise, the transition is a crossover, if the order parameter is continuous and differentiable.
The solutions of the gap equation, which is solved by the iteration of the right hand side of equation (3.9), are shown in Fig. 3.1 as a function of the chemical potential μ for various temperatures. The left side corresponds to the solutions in the chiral limit and the right one to finite bare quark mass. It can be seen, that in the chiral limit a first order transition changes over to a second order transition at a certain critical point $(T_{\text{c}},\ \mu_{\text{c}}) \approx (69.7\ \text{MeV},\ 272.85\ \text{MeV})$, since the effective mass becomes discontinuous for low temperatures ($T < 80$ MeV). In contrast, in the case with finite bare quark mass, the first order transition turns into a crossover, wherein the effective mass falls smoothly down to a finite value. This indicates that the chiral symmetry is only approximately fulfilled.

The global minimum can be obtained by looking at the thermodynamic potential depicted in Fig. 3.2. In the chiral limit (left figure), the thermodynamic potential is symmetric under transposition of M_0 and $-M_0$. For $\mu < 300$ MeV, it has two minima at $M_0 = M_{\text{vac}} = 300$ MeV and $M_0 = -M_{\text{vac}}$, and a maximum at $M_0 = 0$ MeV. At $\mu \approx 300.6$ MeV, the maximum turns into a minimum and with increasing chemical potential it becomes the favored solution. The thermodynamic potential, which incorporates the bare quark mass (right figure), shares the same behavior, but with two differences. It is no more symmetric

like in the chiral limit, precisely the negative solutions are always disfavored and the minimum for high chemical potentials is shifted from zero to the bare quark mass.

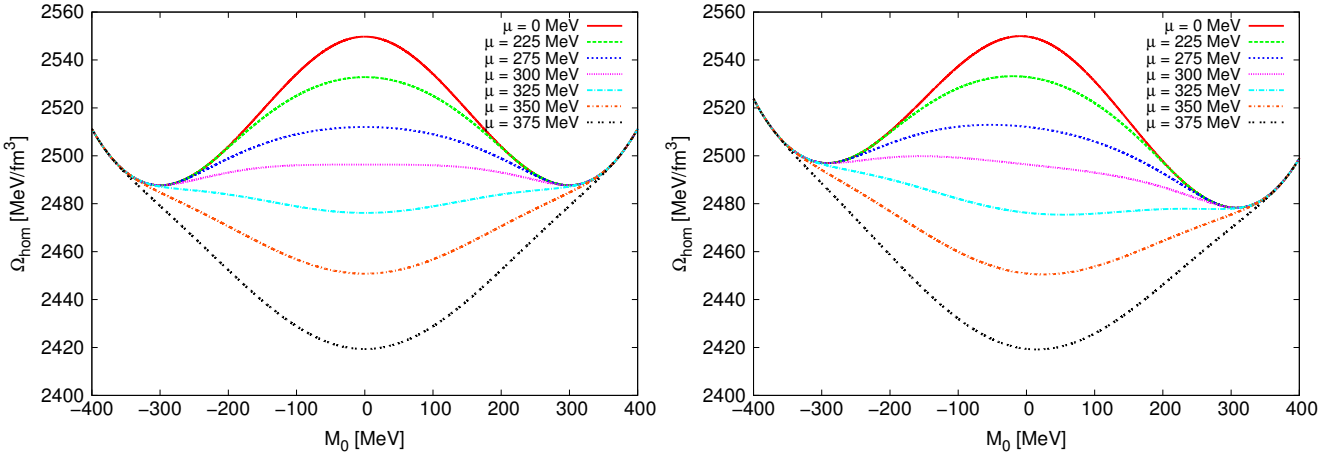

Figure 3.2: Thermodynamic potential Ω_{hom} in homogeneous case over the effective mass M_0 at $T = 0$ MeV for several chemical potentials. Left: chiral limit. Right: finite bare quark mass $m = 5$ MeV.

3.2 Phase diagram

In the phase diagram, depicted in Fig. 3.3, all phase transitions are summarized in the $\mu - T$ plane. The phase boundaries, denoted by solid/dashed lines for the first/second order transition, separate the chirally broken (left) from the restored phase (right), while on the phase boundaries both phases coexist. The first order transition proceeds up to the critical point (marked by a dot). From the critical point upwards, a second order transition in the chiral limit (or a crossover in the case with finite bare quark mass) occurs and ends at $(T,\ \mu) = (165.7\ \text{MeV},\ 0\ \text{MeV})$.

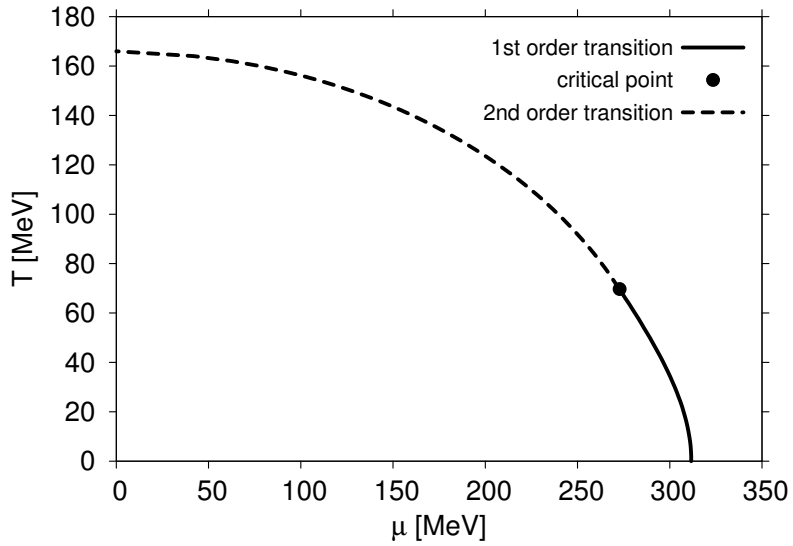

Figure 3.3: Phase diagram in the chiral limit. The first/second order transition is denoted by solid/dashed lines. The black dot is the critical point at $(T_c,\ \mu_c) \approx (69.7\ \text{MeV},\ 272.85\ \text{MeV})$.

4 One-dimensional modulations

4.1 General

In this thesis we want to focus on one-dimensional modulations in the mass ansatz to simplify the numerical calculations:

$$M(z) = \sum_n M_n e^{inqz} \text{ with } n \in \mathbb{Z} \tag{4.1}$$

Thereby the Brillouin zone is finite in the direction of the modulation momentum $\vec{q} = (0,0,q)^T$, but infinite in the plane orthogonal to $\vec{q}$. This allows us to reduce the demanding numerical computation of the eigen system of the Hamiltonian by using the Lorentz symmetry. This powerful technique was already developed by D. Nickel [17] and in the following, we will recap the important steps behind that method.
In general, the Hamiltonian H^+ depends on the momenta $\vec{p}$. The basic idea is now to split the momenta $\vec{p}$ into parallel (longitudinal) and orthogonal (transverse) parts with respect to the direction of the quark condensate modulation. Explicitly, we define

$$\vec{p} = \vec{p}_\parallel + \vec{p}_\perp \tag{4.2}$$

$$\vec{p}_\parallel \equiv (\vec{p}\vec{q})\ \frac{\vec{q}}{|\vec{q}|^2} \tag{4.3}$$

$$\vec{p}_\perp \equiv \vec{p} - \vec{p}_\parallel. \tag{4.4}$$

Since we will work with a condensate, which varies only in the longitudinal direction, the transverse momenta $\vec{p}_\perp$ should not change. Therefore the corresponding transverse momentum operator $\vec{P}_\perp$ commutes with the Hamiltonian H^+, and both operators exhibit simultaneous eigenstates $|E_\lambda, \vec{p}_\perp\rangle$, denoted by the energy E_λ and the transverse momentum $\vec{p}_\perp$. So we can now consider the frame $\vec{p}_\perp = \vec{0}$ and solve the dimensionally reduced eigenvalue problem

$$H^+ |\lambda, \vec{0}\rangle = \lambda |\lambda, \vec{0}\rangle . \tag{4.5}$$

Through a Lorentz transformation $\Lambda^\mu{}_\nu$, we can boost the reduced eigenvalues λ to the eigenvalues E_λ of the full 3+1 dimensional system:

$$\begin{pmatrix} E_\lambda \\ \vec{p} \end{pmatrix}^\mu = \begin{pmatrix} \lambda \cdot \sqrt{1 + \vec{p}_\perp^{\,2}/\lambda^2} \\ \vec{p}_\perp + \vec{p}_\parallel \end{pmatrix}^\mu = \Lambda^\mu{}_\nu \begin{pmatrix} \lambda \\ \vec{p}_\parallel \end{pmatrix}^\nu \tag{4.6}$$

If the modulation momentum is restricted to the third direction $\vec{q} = (0,0,q)^T$, the Hamiltonian momentum components take the following form:

$$H^{+,1\mathrm{D}}_{p,p'} = \gamma^0\gamma^3 p_z \delta_{p,p'} + \gamma^0 P_+ \sum_n M_n \delta_{p,p'+nq} + \gamma^0 P_- \sum_n M_n^* \delta_{p,p'-nq} \tag{4.7}$$

$$= \begin{pmatrix} -p_z\delta_{p,p'} & 0 & \sum_n M_n \delta_{p,p'+nq} & 0 \\ 0 & p_z\delta_{p,p'} & 0 & \sum_n M_n \delta_{p,p'+nq} \\ \sum_n M_n^* \delta_{p,p'-nq} & 0 & p_z\delta_{p,p'} & 0 \\ 0 & \sum_n M_n^* \delta_{p,p'-nq} & 0 & -p_z\delta_{p,p'} \end{pmatrix} \tag{4.8}$$

With a unitary transformation in Dirac space

$$U = \frac{1}{2}\left[-\gamma^0 P_+ \left(\gamma^1 - i\gamma^2\right) + P_- \left(\gamma^1 + i\gamma^2\right) + \left(\gamma^0 P_- + P_+\right)\left(\mathbb{1} + \gamma^3\right)\right] = \begin{pmatrix} 0 & 0 & 0 & 1 \\ 1 & 0 & 0 & 0 \\ 0 & 0 & 1 & 0 \\ 0 & 1 & 0 & 0 \end{pmatrix} \tag{4.9}$$

the above Hamiltonian can be block diagonalized

$$H^{+,1\mathrm{D}}_{p,p'} = U^\dagger \left(H^{\mathrm{BdG},+}_{p,p'} \oplus H^{\mathrm{BdG},-}_{p,p'} \right) U. \tag{4.10}$$

The Bogoliubov-de Gennes (BdG) Hamiltonians $H^{\mathrm{BdG},\pm}_{p,p'}$ given by

$$H^{\mathrm{BdG},+}_{p,p'} = \sigma^3 p_z \delta_{p,p'} + \frac{1}{2}\left(\sigma^1 + i\sigma^2\right) \sum_n M_n \delta_{p,p'+nq} + \frac{1}{2}\left(\sigma^1 - i\sigma^2\right) \sum_n M_n^* \delta_{p,p'-nq} \tag{4.11}$$

$$= \begin{pmatrix} p_z \delta_{p,p'} & \sum_n M_n \delta_{p,p'+nq} \\ \sum_n M_n^* \delta_{p,p'-nq} & -p_z \delta_{p,p'} \end{pmatrix} \tag{4.12}$$

$$H^{\mathrm{BdG},-}_{p,p'} = \sigma^3 p_z \delta_{p,p'} + \frac{1}{2}\left(\sigma^1 + i\sigma^2\right) \sum_n M_n^* \delta_{p,p'-nq} + \frac{1}{2}\left(\sigma^1 - i\sigma^2\right) \sum_n M_n \delta_{p,p'+nq} \tag{4.13}$$

$$= \begin{pmatrix} p_z \delta_{p,p'} & \sum_n M_n^* \delta_{p,p'-nq} \\ \sum_n M_n \delta_{p,p'+nq} & -p_z \delta_{p,p'} \end{pmatrix} \tag{4.14}$$

appear in a wide range in the theoretical physics e.g. crystalline condensates in the chiral Gross-Neveu (GN) model [31], theory of ultra cold Fermi gases [32]. For more information on the mathematical properties of the BdG Hamiltonian, we refer to [33]. Since both Hamiltonians can be transformed into one another by

$$H^{\mathrm{BdG},+} = -A^\dagger H^{\mathrm{BdG},-} A \tag{4.15}$$

with a unitary matrix $A_{p,p'} = i\sigma^2 \delta_{p,p'}$, we will use the eigenvalues of $H^{\mathrm{BdG},+}$ and denote them with λ_{BdG}. The kinetic part of the thermodynamic potential can now be obtained by projecting the longitudinal momentum into the first Brillouin zone and substituting the energy eigenvalues E_λ in (2.73) by $\mathrm{sign}(\lambda_{\mathrm{BdG}}) \cdot \sqrt{\lambda^2_{\mathrm{BdG}} + p_\perp^2}$:

$$\begin{aligned} \Omega_{\mathrm{kin}} = &-\frac{N_{\mathrm{c}} N_{\mathrm{f}}}{(2\pi)^2} \int_0^q \mathrm{d}k_{\mathrm{z}} \int_0^\infty \mathrm{d}p_\perp \, p_\perp \times \\ &\times \sum_{\lambda_{\mathrm{BdG}}} \left\{ \sum_{j=0}^{3} c_j \cdot \sqrt{\lambda^2_{\mathrm{BdG}}(k_z) + p_\perp^2 + j\Lambda^2} + T \sum_{s\in\{-1,1\}} \ln\left[1 + \exp\left(-\frac{\sqrt{\lambda^2_{\mathrm{BdG}}(k_z) + p_\perp^2} - s\mu}{T} \right) \right] \right\} \end{aligned} \tag{4.16}$$

Note, the relation (4.15) implies that the negative eigenvalues of $H^{\mathrm{BdG},+}$ are the positive ones [6] of $H^{\mathrm{BdG},-}$. Therefore, we have to sum over all eigenvalues of $H^{\mathrm{BdG},+}$ and take the absolute value of them. This boosting procedure has two technical advantages: the Hamiltonian $H^{\mathrm{BdG},+}$ has a simpler structure (less off-diagonals) than H^+ and the integration in (4.16) over the transversal momentum $p_\perp$ can be performed analytically

$$\begin{aligned} \Omega_{\mathrm{kin}} = &\frac{N_{\mathrm{c}} N_{\mathrm{f}}}{(2\pi)^2} \int_0^q \mathrm{d}k_{\mathrm{z}} \sum_{\lambda_{\mathrm{BdG}}} \left(\sum_{j=0}^{3} \frac{c_j}{3} \cdot \left(\lambda^2_{\mathrm{BdG}} + j\Lambda^2 \right)^{3/2} + \right. \\ &\left. + \sum_{s\in\{-1,1\}} \begin{cases} T^2 \left[|\lambda_{\mathrm{BdG}}| \cdot \mathrm{Li}_2\left(-e^{-\frac{1}{T}\left(|\lambda_{\mathrm{BdG}}| - s\mu\right)} \right) + T\,\mathrm{Li}_3\left(-e^{-\frac{1}{T}\left(|\lambda_{\mathrm{BdG}}| - s\mu\right)} \right) \right] & \text{if } T > 0 \\ \frac{1}{6}\theta\left(s\mu - |\lambda_{\mathrm{BdG}}|\right) \cdot \left[s\mu\left(\mu^2 - 3\lambda^2_{\mathrm{BdG}}\right) + 2|\lambda_{\mathrm{BdG}}|^3 \right] & \text{if } T = 0 \end{cases} \right) \end{aligned} \tag{4.17}$$

[6] This can be easily seen by applying the eigenvalue relation on (4.15).

with the polylogarithm $\mathrm{Li}_n(z)$ defined by

$$\mathrm{Li}_n(z) = \sum_{k=1}^{\infty} \frac{z^k}{k^n}. \tag{4.18}$$

Finally, the gap equations follow from the boosted thermodynamic potential above:

$$\begin{aligned} M_n - m\delta_{n,0} = &-\frac{4N_c N_f g_s}{(2\pi)^2} \int_0^q \mathrm{d}k_z \sum_{\lambda_{\mathrm{BdG}}} \lambda_{\mathrm{BdG}} \frac{\partial \lambda_{\mathrm{BdG}}}{\partial M_n^*} \times \\ &\times \left(\sum_{j=0}^{3} c_j \cdot \sqrt{\lambda_{\mathrm{BdG}}^2 + j\Lambda^2} + \sum_{s\in\{-1,1\}} \begin{cases} T \ln\left[1 + \exp\left(-\frac{|\lambda_{\mathrm{BdG}}| - s\mu}{T}\right)\right] & \text{if } T > 0 \\ \theta\left(s\mu - |\lambda_{\mathrm{BdG}}|\right) \cdot \left(s\mu - |\lambda_{\mathrm{BdG}}|\right) & \text{if } T = 0 \end{cases} \right) \end{aligned} \tag{4.19}$$

with

$$\frac{\partial \lambda_{\mathrm{BdG}}}{\partial M_n^*} = \omega_{\lambda_{\mathrm{BdG}}}^{\dagger} \frac{\partial H^{\mathrm{BdG},+}}{\partial M_n^*} \omega_{\lambda_{\mathrm{BdG}}} = \sum_p \left(\omega_{\lambda_{\mathrm{BdG}}}^{+}\right)_p^{\dagger} \left(\omega_{\lambda_{\mathrm{BdG}}}^{-}\right)_{p+nq} \tag{4.20}$$

and

$$\omega_{\lambda_{\mathrm{BdG}}}^{\pm} := \frac{1}{2}\left(\sigma^1 \pm i\sigma^2\right) \omega_{\lambda_{\mathrm{BdG}}} \tag{4.21}$$

where $\omega_{\lambda_{\mathrm{BdG}}}$ are the eigenvectors of $H^{\mathrm{BdG},+}$. To solve the gap equations, a numerical diagonalization of the Hamiltonian is required, which however is very time-consuming. We will reduce the computation time by using the asymptotic density of states [17], described in App. E.

4.2 Chiral density wave

Some interesting properties of the inhomogeneous phases can already be studied with only one Fourier component ($M_1 \in \mathbb{R}$) in the mass ansatz, which is called "chiral density wave" (CDW) and describes a spiral in the complex plane:

$$M(z) = M_1 \, e^{iqz} \tag{4.22}$$

In this case analytic eigenvalues of the corresponding Hamiltonian $H^{\mathrm{BdG},+}$ can be determined. This leads to the following gap equation (see App. F for details)

$$M_1 = -\frac{2N_c N_f}{(2\pi)^2} g_s M_1 \int_{-\infty}^{\infty} \mathrm{d}k_z \frac{1}{\sqrt{k_z^2 + M_1^2}} \left[\lambda_{\mathrm{CDW}}^{+}(k_z) \cdot \tilde{g}\left(\lambda_{\mathrm{CDW}}^{+}(k_z)\right) + \lambda_{\mathrm{CDW}}^{-}(k_z) \cdot \tilde{g}\left(\lambda_{\mathrm{CDW}}^{-}(k_z)\right)\right] \tag{4.23}$$

with the eigenvalues

$$\lambda_{\mathrm{CDW}}^{\pm}(k_z) = \sqrt{k_z^2 + M_1^2} \pm \frac{q}{2} \tag{4.24}$$

and

$$\tilde{g}(\lambda_{\mathrm{CDW}}^{\pm}) = \sum_{j=0}^{3} c_j \cdot \sqrt{(\lambda_{\mathrm{CDW}}^{\pm})^2 + j\Lambda^2} + \sum_{s\in\{-1,1\}} \begin{cases} T \ln\left[1 + \exp\left(-\frac{|\lambda_{\mathrm{CDW}}^{\pm}| - s\mu}{T}\right)\right] & \text{if } T > 0 \\ \theta\left(s\mu - |\lambda_{\mathrm{CDW}}^{\pm}|\right) \cdot \left(s\mu - |\lambda_{\mathrm{CDW}}^{\pm}|\right) & \text{if } T = 0 \end{cases}. \tag{4.25}$$

The solutions of the gap equation are obtained by fixed-point iteration and minimizing the corresponding thermodynamic potential with respect to q. The numerical integration was done with the QAGS algorithm from GSL [30] with a numerical boundary cutoff of order 100 GeV due to the bad convergence of the integrals at high energies.
Fig. 4.1 shows the first Fourier component M_1 and the modulation momentum q as a function of the chemical potential at $T = 0$ MeV. The consideration of a spatially dependent condensate leads to three different regions. The chirally broken phase ($M_1 = 300$ MeV$, q = 0$) exists up to certain critical value $\mu_{c,1}, \approx 310.4$ MeV and goes into the inhomogeneous phase with a non-zero q by a first order transition. With increasing μ, the mass amplitude decreases, while the modulation momentum rises. At $\mu_{c,2} \approx 344.8$ MeV the inhomogeneous phase turns into the restored phase via a second order transition with a zero mass coefficient, whereas the modulation momentum becomes irrelevant.

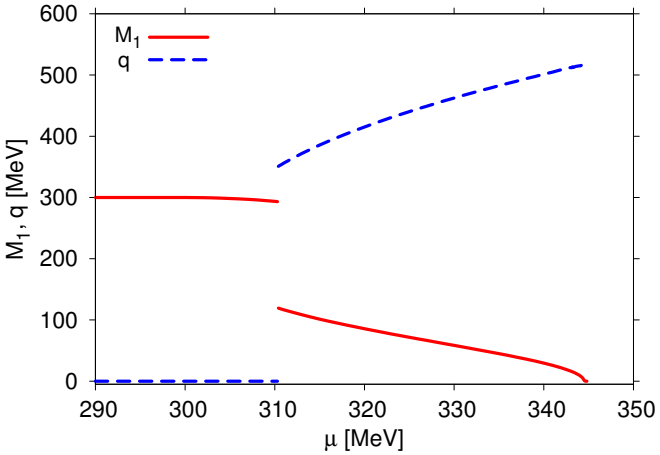

Figure 4.1: The modulation momentum q and first mass coefficients M_1 over chemical potential μ at $T = 0$ MeV.

4.3 Gap equations for three mass coefficients

Here, we consider the Fourier ansatz with three real Fourier coefficients:

$$M(z) = \sum_{n=-1}^{1} M_n e^{inqz} = M_0 + M_{-1} e^{-iqz} + M_1 e^{iqz} \tag{4.26}$$

This ansatz corresponds to two plane waves with opposite direction and different amplitudes plus an overall shift and can be considered as a generalization of the CDW case. So, taking this ansatz into account, the momentum components of the Hamiltonian read

$$\begin{aligned} H^{\mathrm{BdG},+}_{p,p'} &= \sigma^3 p_z \delta_{p,p'} + \sigma^1 M_0 \delta_{p,p'} + \\ &+ \left[\frac{1}{2}\left(\sigma^1 + i\sigma^2\right) M_{-1} + \frac{1}{2}\left(\sigma^1 - i\sigma^2\right) M_1\right] \delta_{p,p'-q} + \left[\frac{1}{2}\left(\sigma^1 + i\sigma^2\right) M_1 + \frac{1}{2}\left(\sigma^1 - i\sigma^2\right) M_{-1}\right] \delta_{p,p'+q}. \end{aligned} \tag{4.27}$$

Since the Hamiltonian is infinite in momentum space, we have to limit the momentum space by a numerical cutoff. In general, the cutoff should be chosen large enough, so that boundary effects could be neglected. Instead of applying a hard cutoff to the Hamiltonian matrix, we will take advantage of the asymptotic behavior of the spectral density (see App. E for details).

The general form of the Hamiltonian (4.12) has a sparse banded structure (since the Pauli matrices expand the non-zero diagonals). Explicitly for three Fourier components, the Hamiltonian matrix takes the form

$$H^{\mathrm{BdG},+}(k_z) = \begin{pmatrix} D_{-N}(M_0) & O(M_1, M_{-1}) & \mathbb{O}_{2\times2} & \cdots & \mathbb{O}_{2\times2} \\ O(M_{-1}, M_1,) & D_{-N+1}(M_0) & \ddots & \ddots & \vdots \\ \mathbb{O}_{2\times2} & \ddots & \ddots & \ddots & \mathbb{O}_{2\times2} \\ \vdots & \ddots & \ddots & D_{N-1}(M_0) & O(M_1, M_{-1}) \\ \mathbb{O}_{2\times2} & \cdots & \mathbb{O}_{2\times2} & O(M_{-1}, M_1,) & D_N(M_0) \end{pmatrix} \tag{4.28}$$

with the 2×2 matrix blocks

$$D_r(M_0) = \sigma^3(k_z + rq) + \sigma^1 M_0 = \begin{pmatrix} k_z + rq & M_0 \\ M_0 & -(k_z + rq) \end{pmatrix},\ r \in \mathbb{Z} \tag{4.29}$$

$$O(M_{\pm1}, M_{\mp1}) = \frac{1}{2}\left(\sigma^1 + i\sigma^2\right) M_{\mp1} + \frac{1}{2}\left(\sigma^1 - i\sigma^2\right) M_{\pm1} = \begin{pmatrix} 0 & M_{\mp1} \\ M_{\pm1} & 0 \end{pmatrix}. \tag{4.30}$$

Furthermore, the momentum cutoff $\Lambda_{\vec{p}} \geq |k_z + Nq|$ and the modulation momentum q determine the maximal size of the Hamiltonian matrix in momentum space by

$$N = \lfloor |\Lambda_{\vec{p}} - k_z| / q \rfloor \tag{4.31}$$

where $\lfloor x \rfloor$ is the floor function, which gives the largest integer less than or equal to x, so that the maximal size of the Hamiltonian is given by $2 \cdot (2N + 1)$.
The corresponding gap equations (2.75) can be written in a compact notation:

$$\vec{M} = 4 g_s N_c N_f \vec{h}\left(\vec{M}\right) + m\vec{e}_2 \tag{4.32}$$

with

$$\vec{M} = (M_{-1},\ M_0,\ M_1)^T \tag{4.33}$$

$$\vec{h} = (h_{-1},\ h_0,\ h_1)^T \tag{4.34}$$

$$\vec{e}_2 = (0,\ 1,\ 0)^T \tag{4.35}$$

and

$$h_n\left(\vec{M}\right) = \frac{-1}{(2\pi)^2} \int_0^q \mathrm{d}k_z \sum_{\lambda_{\mathrm{BdG}}} \lambda_{\mathrm{BdG}} \cdot \left(\sum_p \left(\omega^+_{\lambda_{\mathrm{BdG}}}\right)^\dagger_p \left(\omega^-_{\lambda_{\mathrm{BdG}}}\right)_{p+nq} \right) \times$$
$$\times \left(\sum_{j=0}^{3} c_j \cdot \sqrt{\lambda^2_{\mathrm{BdG}} + j\Lambda^2} + \sum_{s\in\{-1,1\}} + T \ln\left[1 + \exp\left(-\frac{|\lambda_{\mathrm{BdG}}| - s\mu}{T} \right) \right] \right). \tag{4.36}$$

To solve them, one can iterate the right hand side of equation (4.32) up to a certain precision. After inserting the solutions of the iterated gap equations into the thermodynamic potential, calculated for different modulation momenta, the remaining parameter q can be obtained by the minimization of Ω. The numerical diagonalization of the Hamiltonian matrix was performed with the divide and conquer algorithm (DSBEVD routine) of the LAPACK library [34].

5 Numerical results

In the following we want to give an example of the behavior of the Fourier coefficients as a function of the iteration steps before we present the results for various chemical potentials. In Fig. 5.1 are illustrated the amplitudes over the number of iterations with initial values from the CDW case for $T = 0$ and $\mu = 325$ MeV (inhomogeneous region). In the chiral limit (left picture), all coefficients remain on their initial values over the whole iteration range. This shows that the CDW ansatz is self-consistent. In contrast to that, a non-vanishing bare quark (right picture) leads to a rise of the zero component M_0 from zero to a finite value $M_0 = 55.90$ MeV. After 260 iterations, it drops slightly to 55.192 MeV and does not change drastically with further iterations. Otherwise, the M_1 component declines and M_{-1} increases until both reach the same value $M_{-1} \approx M_1 = 66.40$ MeV after 271 iterations. Hence, the Fourier ansatz becomes a cosine plus a constant shift.

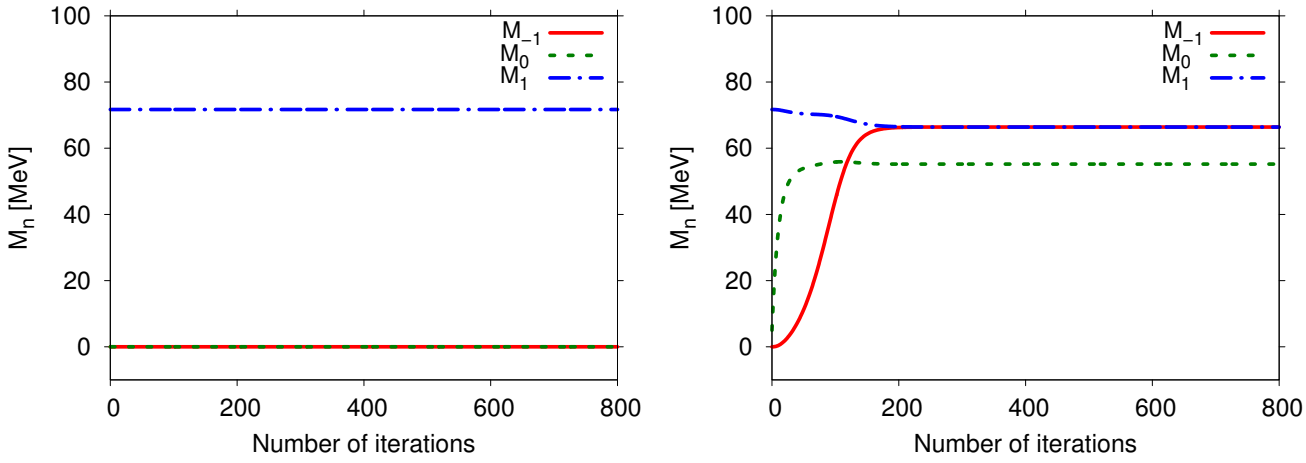

Figure 5.1: The mass coefficients M_n over the number of iteration steps in the chiral limit (left) and with finite current quark mass $m = 5$ MeV (right) for $T = 0$ and $\mu = 325$ MeV. As initial values for the iterations, we chose the parameters from the CDW case: $q = 440.22$ MeV, $M_1^{\text{init}} = 71.70$ MeV and $M_0^{\text{init}} = M_{-1}^{\text{init}} = 0$.

On the other hand, if we set a finite initial value for the first minus component in the chiral limit, e.g. $M_{-1}^{\text{init}} = 20$ MeV, the M_{-1} and M_1 components converge to the same value as shown in Fig. 5.2. We found out that the absolute values of the mirrored coefficients M_{-i} and M_i for $i > 0$ are equal in the case of higher amplitudes up to order seven, too. The solutions with different signs of the mirrored components are the local minima of the thermodynamic potential and therefore are not considered, while solutions with unequal absolute values for the mirrored coefficients were not found. We also tried to generate other solutions for higher coefficients by using the parameters (coefficients and modulation momentum) from the gap equation system with lower components. The same results can also be obtained by minimizing the thermodynamic potential with respect to the higher coefficients. Accordingly, we did not find new solutions. Therefore, we will present in the following sections the favored solutions, which were mentioned above ($M_i = M_{-i}$).

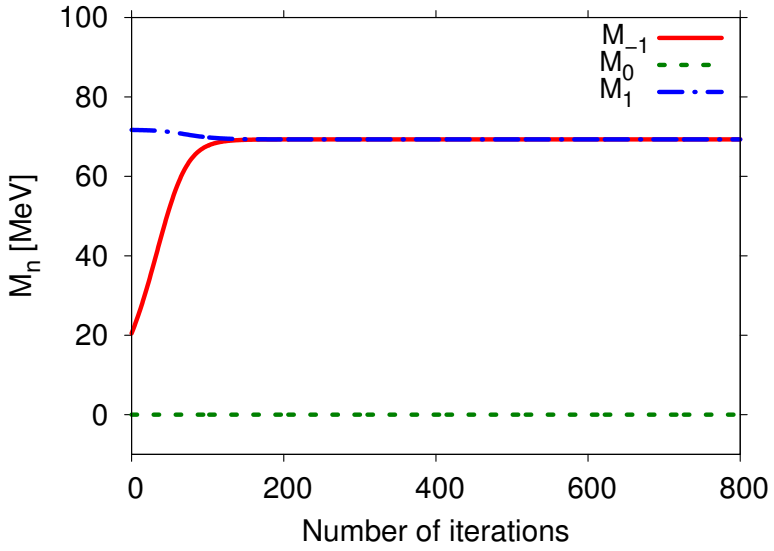

Figure 5.2: The mass coefficients M_n over the number of iterations in the chiral limit for $T = 0$ and $\mu = 325$ MeV. The initial values are same as in Fig. 5.1 except for the first minus component: $M_{-1}^{\text{init}} = 20$ MeV.

5.1 Three coefficients

The results of three mass coefficients and the modulation momentum are depicted in Fig. 5.3 over the chemical potential. Again, we can identify three different regions in the chiral: the chirally broken phase, the inhomogeneous phase, and the chirally restored phase. The gap coefficients in the chirally broken phase can not be obtained directly with the numerical diagonalization procedure, since the favored solution $q = 0$ in this phase will lead to an infinite Hamiltonian. However, at a certain chemical potential, the inhomogeneous solution is disfavored against the homogeneous one. Thus, this point can be determined by the intersection of the homogeneous with the inhomogeneous thermodynamic potential shown in Fig. 5.7. In the chiral limit, we found that the inhomogeneous phase sets in through a first order transition at $\mu \approx 308.53$ MeV and ends at $\mu \approx 344.4$ MeV with a second order transition into the chirally restored phase. The mass coefficients M_1 and M_{-1} are equal and show the same behavior like in the CDW case with the exception of the onset of the inhomogeneous phase, which occurs at smaller chemical potential than with the CDW ansatz. The Fourier component M_0 is zero in the inhomogeneous as well as in the chirally restored region. So, even if we assume a complex mass modulation $M(\vec{x})$, the Fourier components adjust themselves so, that the pseudoscalar condensate ϕ_P^3 disappears and the effective mass modulation reduces to the known sinusoidal ansatz [19,35]. This suggests that only real solutions are favored, which was already stated in [17] with the Ginzburg-Landau (GL) approach in the NJL model.

In the case of a finite current quark mass (right side of Fig. 5.3), there are only two phases in the strict sense: the homogeneous broken and the inhomogeneous phase. This is due the fact that an exact order parameter does not exist for the distinction between the homogeneous broken and the chirally restored phase. Nevertheless, the behavior of M_1 and M_{-1} stays the same as in the chiral limit. However, the influence of the current quark mass results in a smaller inhomogeneous window (that starts at $\mu = 320.93$ MeV and ends at $\mu = 345.2$ MeV) and a finite zero coefficient M_0 in the inhomogeneous region. In this region, all coefficients decline with a rising modulation momentum, whereas the zero coefficient takes a slightly lesser value than the other two for $\mu < 341$ MeV. Outside the inhomogeneous region ($\mu > 345.2$ MeV), where the modulation momentum is undetermined, M_{-1} and M_1 are zero, while M_0 still remains finite.

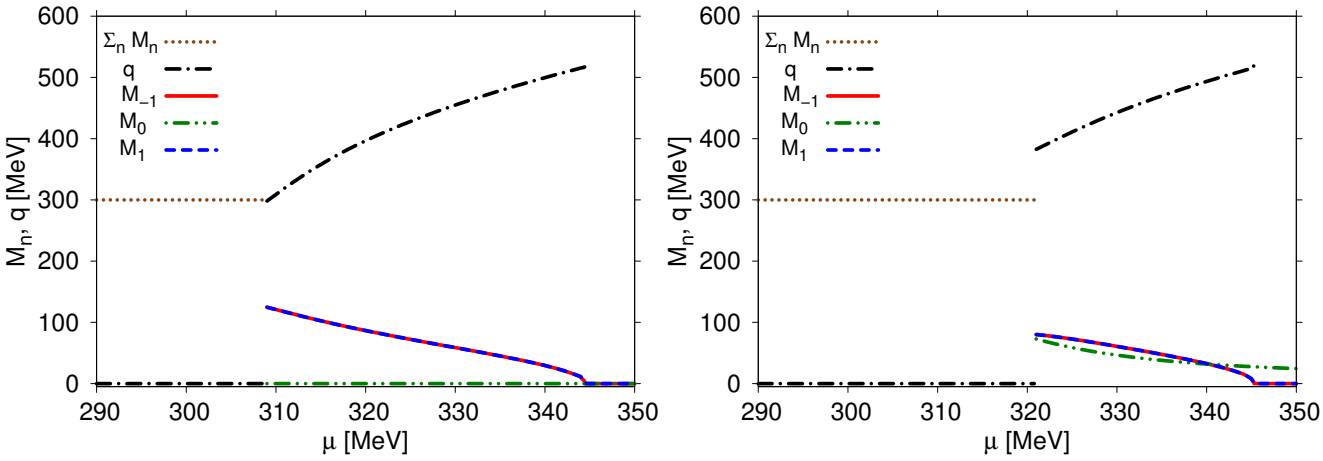

Figure 5.3: The mass coefficients M_n and the modulation momentum q over the chemical potential μ at $T = 0$ MeV, $m = 0$ MeV (left side) and $m = 5$ MeV (right side). In the homogeneous region the mass ansatz reduces to a sum of all coefficients due to a zero modulation momentum.

The corresponding phase diagram is presented in Fig. 5.4. In the chiral limit, the inhomogeneous region is enclosed by the first order transition (black dashed line) from the homogeneous chirally broken to the inhomogeneous phase and the second order transition (red dashed line) from the inhomogeneous to

the chirally restored phase. Between the both phase transitions lies the first order transition (black solid line) of the homogeneous phase, which is shown for comparison. All three lines meet at a Lifschitz point (LP), which coincides with the critical point of the homogeneous phase diagram. Although the Lifschitz point is defined by the intersection of three phase boundaries of second-order, it is also common to use this notion for the intersection of three phase boundaries, which do not fulfill this condition.

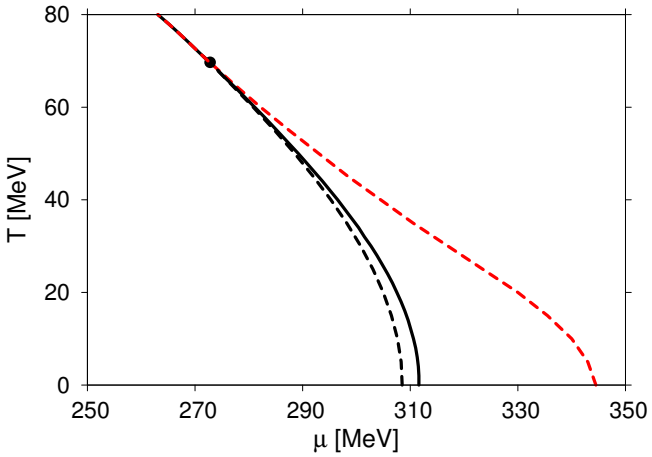

Figure 5.4: Phase diagram for the Fourier ansatz with three mass coefficients in the chiral limit. The black/red dashed line indicates the first/second order transition, while the solid black line shows the first order transition of the homogeneous phase. The Lifschitz point is marked by the black dot.

5.2 Seven coefficients

To check the self-consistency of the gap equation system, we include the higher amplitudes $M_{\pm 2}$ and $M_{\pm 3}$ in our ansatz. It turned out that the Fourier ansatz is only self-consistent if the gap system is restricted to the CDW case. Otherwise, a non-zero initial value for $M_{\pm 1}$ gives a small contribution to $M_{\pm 3}$ in the chiral limit and in addition a finite bare quark affects the values of the even mass coefficients $M_0, M_{\pm 2}$. This can be seen in Fig. 5.5, where only the sum of the mirrored components M_{-i} and M_i for $i > 0$ are shown, since each of them yields the same value (with a numerical uncertainty of 10^{-3} MeV). The subdivision of the phases with zero as well as with finite current quark mass is the same as in the three coefficients case. In the chiral limit (left side of Fig. 5.5) the plus and minus first components provide the largest contributions, while the plus and minus third coefficients exhibit small negative values only at the onset of the inhomogeneous region. All even amplitudes are zero, which also stays true if we include higher coefficients (see next section). The situation changes if we consider a non-vanishing bare quark mass (right side of Fig. 5.5): the components $M_{\pm 2}$ get negative minor contributions at the vicinity of the first order transition. Since the onset of the inhomogeneous window shifts to higher chemical potentials, the value of the odd coefficients $M_{\pm 3}$ is close to zero.
Overall, the seven coefficients case has a weaker first order transition between the homogeneous broken and the inhomogeneous phase than for three coefficients, since the modulation momentum reaches lower values. This due to fact that the Fourier ansatz can be considered as a kind of the generalization of the solitonic solution (see section 5.3). The Fourier shape approaches the solitonic shape by including higher amplitudes. Thus, the first order transition approaches a second order transition, which only occurs in the solitonic case.

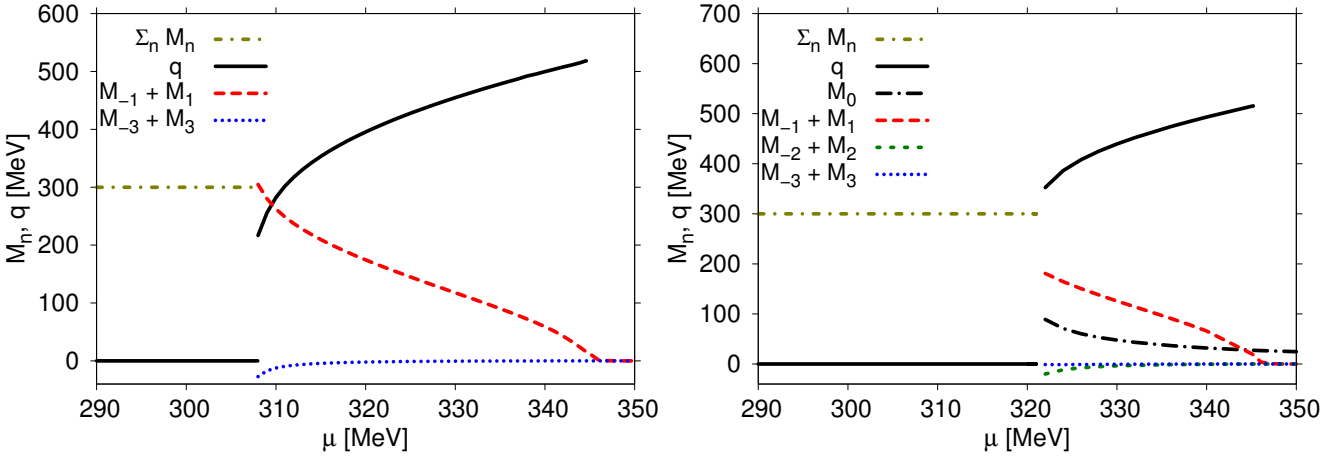

Figure 5.5: The sum of the mirrored mass coefficients $M_{-i} + M_i$ and the modulation momentum q are plotted over the chemical potential μ at $T = 0$ MeV, respectively in the chiral limit (left) and with finite bare quark mass $m = 5$ MeV (right). In the chiral limit all even amplitudes vanish and therefore are not displayed.

5.3 Higher coefficients

In the following we want to compare the Fourier ansatz up to the seventh amplitude

$$M(z) = \sum_{n=-7}^{7} M_n \cdot e^{inqz} \tag{5.1}$$

in the chiral limit with the solitonic solution, which is a self-consistent solution to one-dimensional modulations, based on the analytic eigenvalue spectrum of the Hamiltonian of the 1+1-dimensional chiral Gross-Neveu (GN) model. To be more precise, we stated in chapter 4 that the NJL Hamiltonian $H^{+,1D}$ is a direct product of $H^{\mathrm{BdG},+}$ and $H^{\mathrm{BdG},-}$, which correspond to the Hamiltonians of the 1+1-dimensional NJL_2 model. However, the Hamiltonian for real effective mass modulation

$$H^{\mathrm{BdG},+} = H^{\mathrm{BdG},-} = \begin{pmatrix} -i\partial_z & M(z) \\ M(z) & i\partial_z \end{pmatrix} \tag{5.2}$$

presented in position space, is the Hamiltonian of the GN model [36], whose results can be used to construct an analytic expression for the spectral density of $H^{\mathrm{BdG},+}$ as well as for the real mass modulation. The resulting order parameter consists of Jacobi elliptic functions [17]

$$M_{\mathrm{SN}}(z) = \Delta\, \nu \frac{\mathrm{sn}\,(\Delta z|\,\nu)\,\mathrm{cn}\,(\Delta z|\,\nu)}{\mathrm{dn}\,(\Delta z|\,\nu)} \tag{5.3}$$

where ν is elliptic modulus and describes the shape of the modulation and Δ is related to the amplitude. If the elliptic modulus is set to 1, the mass modulation takes the form of a hyperbolic tangent

$$M_{\mathrm{SN}}(z)|_{\nu=1} = \Delta \tanh(\Delta z) \tag{5.4}$$

and therefore forms a 'single kink' (single soliton), which gives the solitonic modulations their name. To compare the Fourier ansatz with the solitonic solution, the mass modulation (5.3) can be expanded numerically in a Fourier series [19]. The coefficients ratios for various chemical potentials are listed in table 5.1. It shows that the Fourier ansatz can be well reproduced (the relative error is less than 6%) by the Fourier decomposition of the Jacobi elliptic functions for $\mu \geq 309.0$ MeV. Only at the onset of the inhomogeneous phases ($\mu < 309.0$ MeV), the difference between the both mass modulations is not negligible (relative error up to 24%). Therefore, the Fourier ansatz is no more a good approximation of the solitonic shape, however, it can be improved by taking more harmonics into account.
Another feature is the vanishing of the even coefficients in addition with similar mirrored coefficients ($M_{-i} \approx M_i$). This implies that the harmonic expansion (5.1) becomes a superposition of cosines. The associated mass modulation in comparison to the solitonic modulation is depicted in Fig. 5.6. While the amplitude of the Fourier and the solitonic modulation is approximately the same, the period of $M(z)$ underestimates the period of $M_{\mathrm{SN}}(z)$. As the chemical potential increases, the amplitude and period decreases in both cases and the profile of $M(z)$ approaches the one of $M_{\mathrm{SN}}(z)$.
All discussed observations are also investigated in the GL approach by Abuki et al. [37] with a similar expansion of the order parameter

$$M(z) = \sum_{n=1,3,5,\ldots} M_n \sin\left((2\pi/L)\, nz\right) \tag{5.5}$$

They come to the conclusion that the solitonic condensate is favored over all 1D modulations.

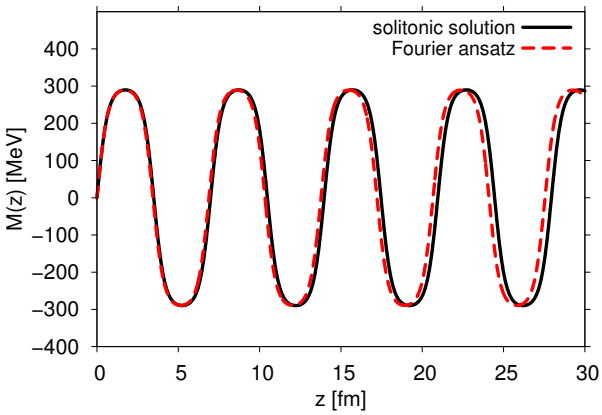

(a) $\mu = 308$ MeV

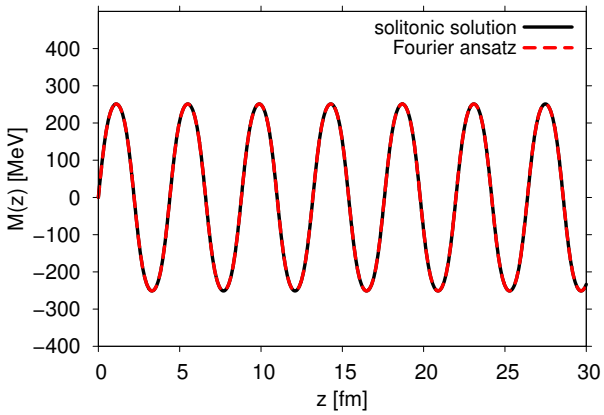

(b) $\mu = 310$ MeV

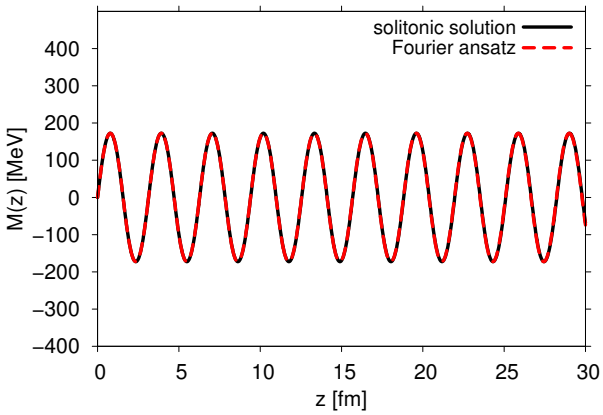

(c) $\mu = 320$ MeV

Figure 5.6: Comparison of the solitonic and the Fourier modulation for various chemical potentials at $T = 0$. The Fourier ansatz were phase shifted by $n\frac{\pi}{2}, n \in \mathbb{N}$ for better comparison, since the solitonic modulation is an odd function. The values for Δ are taken from [38].

	Harmonics of Jacobi elliptic functions			Amplitudes of the Fourier ansatz			
μ [MeV]	$M_3^{\mathrm{SN}}/M_1^{\mathrm{SN}}$	$M_5^{\mathrm{SN}}/M_1^{\mathrm{SN}}$	$M_7^{\mathrm{SN}}/M_1^{\mathrm{SN}}$	q [MeV]	M_3/M_1	M_5/M_1	M_7/M_1
307.5	-0.238386	0.080631	-0.0282258	107.85	-0.223899	0.068786	-0.0213859
308.0	-0.129363	0.019598	-0.0029789	180.00	-0.126516	0.018662	-0.0027523
309.0	-0.062376	0.004167	-0.0002784	253.97	-0.062405	0.004171	-0.0002787
310.0	-0.046727	0.002295	-0.0001128	281.98	-0.046646	0.002287	-0.0001126
315.0	-0.020578	0.000432	-0.0000091	353.25	-0.020647	0.000435	-0.0000092
320.0	-0.011740	0.000132	-0.0000016	395.43	-0.011739	0.000139	-0.0000017

Table 5.1: Comparison of higher harmonics of the Fourier decomposition of the Jacobi elliptic functions, taken from [19], with the Fourier coefficients of the mass ansatz for $T = 0$. The coefficients are divided by the first non-zero amplitude $M_1^{(\mathrm{SN})}$, which provides the largest contribution. It turned out that even coefficients are zero and the coefficients with mirrored indices are equal up to a relative numerical uncertainty of 10^{-3} ($M_{-i} \approx M_i \quad \forall i \in \{1, ..., 7\}$).

5.4 Free energy comparison

From the discussions above, we know that all considered mass modulations are favored over the homogeneous solutions in a certain chemical potential range. To clarify the question which of the crystalline structures are the most favored one, we have to compare the free energies of the different shapes.
In Fig. 5.7, it is visible that the Fourier modulations with higher coefficients are favored over those with fewer ones. This not surprising, since the solitonic solutions, which are expected to be the most favored [18, 19], can be better interpolated by inclusion of higher coefficients, especially in the vicinity of the transition from the homogeneous broken to the inhomogeneous phase. In case of a finite current quark mass, the gap between the thermodynamic potential of the three and the seven coefficients modulation is larger than for the chiral limit. This indicates that the inclusion of higher amplitudes leads to a better approximation of the solitonic solutions with bare quark masses than in the chiral limit. The chiral density wave (complex modulation) is disfavored over all considered modulations in the whole inhomogeneous region.

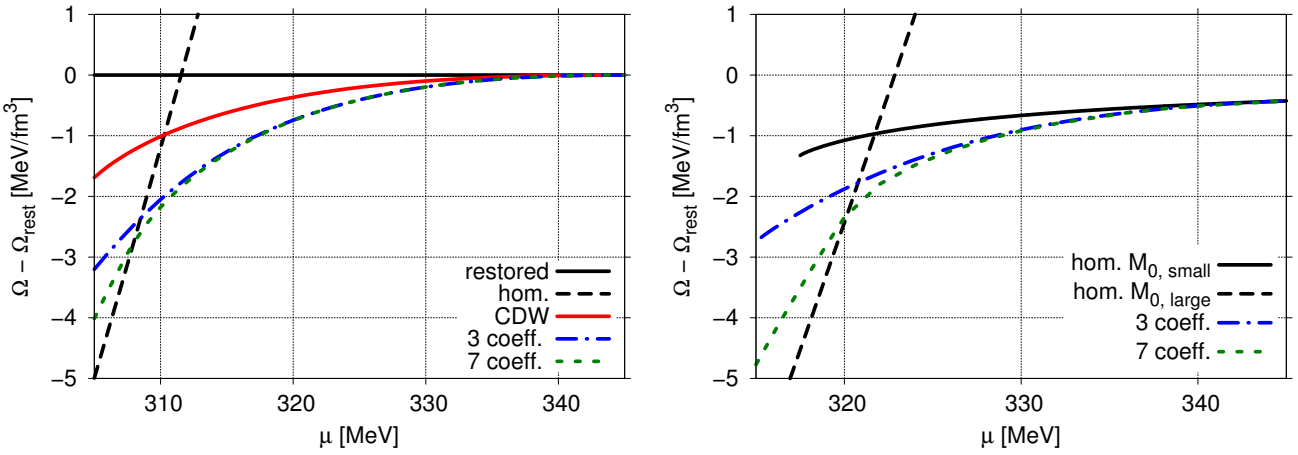

Figure 5.7: Thermodynamic potential minus the restored thermodynamic potential for various mass modulations at $T = 0$ MeV in the chiral limit (left) and with finite current quark mass $m = 5$ MeV (right). The labeling "hom. $M_{0,\text{small/large}}$" refers to the homogeneous solutions for small/large values of M_0 (see Fig. 3.1 r.h.s.).

6 Conclusion and outlook

In this thesis, we introduced the Nambu–Jona-Lasinio model as an effective model for chiral symmetry breaking. We applied the mean-field approximation on the simplest NJL-Lagrangian with scalar and pseudoscalar interaction terms to get the thermodynamic potential in the context of spatially varying condensates. The corresponding Hamiltonian was transformed by using a Fourier expansion for the condensate into momentum space. Since the Hamiltonian matrix is infinite in momentum space, we had to apply a numerical cutoff. The derivation of the thermodynamic potential with respect to the Fourier coefficients led to a system of coupled equations, also called gap equations, where the occurring integrals were rendered to finite values with the energetic version of the Pauli-Villars regularization. After solving the gap equation in the homogeneous case, we considered the mass modulation with one Fourier coefficient (chiral density wave). In addition to a chirally broken and restored phase an inhomogeneous phase with an oscillating solution appeared.
By taking more coefficients into account, we have found that the Fourier modulation reduces to a sum of cosines due to the equal values of the mirrored coefficients. Hence, the case with three mass coefficients in the chiral limit reduces to the well known sinusoidal ansatz, whereas the non-zero bare quark mass leads to a finite zero Fourier component. This suggests that complex modulations are disfavored over the real ones for vanishing and non-vanishing current quark mass. Considering higher coefficients, it has turned out that even coefficients vanish in the chiral limit only. Although, the contributions of higher coefficients are small in comparison to the first ones, they play a crucial role in matters of the approximation of the solitonic modulations. However, the Fourier ansatz is always disfavored against the solitonic solution, especially at the transition of the homogeneous broken to the inhomogeneous phase. A further observation was the reduction of the inhomogeneous region in the case of a finite bare quark mass. Finally, we compared the free energy of the Fourier ansatz for lower coefficients with the one of higher coefficients. Hereby, we found that the free energy of the latter is smaller and therefore favored against the former.
Unfortunately, the goal to construct new solutions for higher amplitudes based on lower amplitudes was not achieved. We only have found the known solutions, which are discovered in previous works or, alternatively, can be obtained by minimization of the thermodynamic potential. The reason for this may be that we have limited ourselves to real coefficients. It would be interesting to see, if the consideration of complex Fourier coefficients will lead to a combination of cosine and sine modulations, or if the imaginary parts in the mass modulation cancel out as in the Fourier ansatz with real components. Furthermore, the comparison between the solitonic and the Fourier modulation with a finite current quark mass has to be done.
The next logical step could be the extension of the gap system to two-dimensional modulations. This will lead not only to more gap equations but also to a more complicated structure of the Hamiltonian. This will result in a significant increasing of the computation time. However, the inclusion of fewer coefficients for two-dimensional modulations may lead to new solutions of the gap equations and could be done in appropriate time.

Appendix

A Conventions

In the whole thesis natural units are used:

$$\hbar = c = k_\mathrm{B} = 1 \tag{A.1}$$

The Minkowski metric is:

$$[\eta]_{\mu\nu} = \mathrm{diag}(1,-1,-1,-1) \tag{A.2}$$

For the gamma matrices, we use the chiral representation

$$\gamma^0 = \begin{pmatrix} 0 & \mathbb{1}_{2\times2} \\ \mathbb{1}_{2\times2} & 0 \end{pmatrix},\ \gamma^k = \begin{pmatrix} 0 & \sigma^k \\ -\sigma^k & 0 \end{pmatrix},\ \gamma^5 = \begin{pmatrix} -\mathbb{1}_{2\times2} & 0 \\ 0 & \mathbb{1}_{2\times2} \end{pmatrix} \tag{A.3}$$

$$\gamma^0\gamma^k = \begin{pmatrix} -\sigma^k & 0 \\ 0 & \sigma^k \end{pmatrix},\ \gamma^0\gamma^5 = \begin{pmatrix} 0 & \mathbb{1}_{2\times2} \\ -\mathbb{1}_{2\times2} & 0 \end{pmatrix} \tag{A.4}$$

with the Pauli matrices:

$$\sigma^1 = \begin{pmatrix} 0 & 1 \\ 1 & 0 \end{pmatrix},\ \sigma^2 = \begin{pmatrix} 0 & -i \\ i & 0 \end{pmatrix},\ \sigma^3 = \begin{pmatrix} 1 & 0 \\ 0 & -1 \end{pmatrix} \tag{A.5}$$

In addition, we define the projectors:

$$P_\pm := \frac{1}{2}\left(1 \pm \gamma^5\right) \tag{A.6}$$

Explicitly, in chiral representation:

$$P_+ = \begin{pmatrix} 0 & 0 \\ 0 & \mathbb{1} \end{pmatrix},\ P_- = \begin{pmatrix} \mathbb{1} & 0 \\ 0 & 0 \end{pmatrix} \tag{A.7}$$

B Integrals

B.1 Calculation of the integral $J_1^{\mathrm{vac}}(M_0)$

The regularized integral $J_1^{\mathrm{vac}}(M_0)$ can be analytically calculated:

$$J_1^{\mathrm{vac}}(M_0) = \int \frac{\mathrm{d}^3\vec{k}}{(2\pi)^3} \sum_{j=0}^{3} c_j \cdot \sqrt{\vec{k}^2 + \mu_j^2} = \frac{2}{(2\pi)^2} \lim_{\lambda\to\infty} \sum_{j=0}^{3} c_j \int_0^\lambda \mathrm{d}|\vec{k}|\ \vec{k}^2\ \sqrt{\vec{k}^2 + \mu_j^2} \tag{B.1}$$

$$= \frac{2}{(2\pi)^2} \lim_{\lambda\to\infty} \sum_{j=0}^{3} c_j \left[\frac{|\vec{k}|}{4}\sqrt{(\vec{k}^2+\mu_j^2)^3} - \frac{\mu_j^2}{8}\left(|\vec{k}|\sqrt{\vec{k}^2+\mu_j^2} + \mu_j^2 \ln\left(|\vec{k}| + \sqrt{\vec{k}^2+\mu_j^2}\right)\right)\right]\Bigg|_0^\lambda \tag{B.2}$$

$$= \frac{2}{(2\pi)^2} \lim_{\lambda\to\infty} \sum_{j=0}^{3} c_j \left[\frac{\lambda}{4}\sqrt{(\lambda^2+\mu_j^2)^3} - \frac{\mu_j^2}{8}\left(\lambda\sqrt{\lambda^2+\mu_j^2} + \mu_j^2 \ln\left(\lambda + \sqrt{\lambda^2+\mu_j^2}\right)\right) + \frac{\mu_j^4}{8}\ln\mu_j \right] \tag{B.3}$$

$$= \frac{1}{8\cdot(2\pi)^2} \sum_{j=0}^{3} c_j \cdot \mu_j^4 \cdot \ln\mu_j^2 \tag{B.4}$$

with

$$\mu_j^2 = M_0^2 + j\Lambda^2 \tag{B.5}$$

C Hamiltonian and inverse propagator in momentum space

C.1 Hamiltonian in momentum space

We get the Hamiltonian in momentum space through a Fourier transformation:

$$H^{\pm}_{\vec{p}_\mathrm{m},\vec{p}_\mathrm{n}} = \frac{1}{V}\int \mathrm{d}^3\vec{x}\; e^{-i\vec{p}_\mathrm{m}\vec{x}} H^{\pm}(\vec{x})\; e^{i\vec{p}_\mathrm{n}\vec{x}} \tag{C.1}$$

$$= \frac{1}{V}\int \mathrm{d}^3\vec{x}\; e^{-i\vec{p}_\mathrm{m}\vec{x}} \left[-i\gamma^0\vec{\gamma}\vec{\nabla} + M^{\pm}(\vec{x})\;\gamma^0 P_+ + M^{\mp}(\vec{x})\;\gamma^0 P_-\right] e^{i\vec{p}_\mathrm{n}\vec{x}} \tag{C.2}$$

$$= \frac{1}{V}\int \mathrm{d}^3\vec{x}\; e^{-i\vec{p}_\mathrm{m}\vec{x}} \left[-i\gamma^0\vec{\gamma}\vec{\nabla} + \sum_{\vec{q}_\mathrm{k}} M^{\pm}_{\vec{q}_\mathrm{k}} e^{\pm i\vec{q}_\mathrm{k}\vec{x}}\gamma^0 P_+ + \sum_{\vec{q}_\mathrm{k}} M^{\mp}_{\vec{q}_\mathrm{k}} e^{\mp i\vec{q}_\mathrm{k}\vec{x}}\;\gamma^0 P_-\right] e^{i\vec{p}_\mathrm{n}\vec{x}} \tag{C.3}$$

$$= \frac{1}{V}\Bigg[\gamma^0\vec{\gamma}\vec{p}_\mathrm{n}\int \mathrm{d}^3\vec{x}\; e^{i(\vec{p}_\mathrm{n}-\vec{p}_\mathrm{m})\vec{x}} +$$

$$+ \sum_{\vec{q}_\mathrm{k}} M^{\pm}_{\vec{q}_\mathrm{k}}\int \mathrm{d}^3\vec{x}\; e^{i\left(\vec{p}_\mathrm{n}-\vec{p}_\mathrm{m}\pm\vec{q}_\mathrm{k}\right)\vec{x}}\gamma^0 P_+ + \sum_{\vec{q}_\mathrm{k}} M^{\mp}_{\vec{q}_\mathrm{k}}\int \mathrm{d}^3\vec{x}\; e^{i\left(\vec{p}_\mathrm{n}-\vec{p}_\mathrm{m}\mp\vec{q}_\mathrm{k}\right)\vec{x}}\gamma^0 P_-\Bigg] \tag{C.4}$$

$$= \gamma^0\vec{\gamma}\vec{p}_\mathrm{n}\delta_{\vec{p}_\mathrm{n},\vec{p}_\mathrm{m}} + \sum_{\vec{q}_\mathrm{k}} M^{\pm}_{\vec{q}_\mathrm{k}}\delta_{\vec{p}_\mathrm{m},\vec{p}_\mathrm{n}\pm\vec{q}_\mathrm{k}}\gamma^0 P_+ + \sum_{\vec{q}_\mathrm{k}} M^{\mp}_{\vec{q}_\mathrm{k}}\delta_{\vec{p}_\mathrm{m},\vec{p}_\mathrm{n}\mp\vec{q}_\mathrm{k}}\gamma^0 P_- \tag{C.5}$$

$$= \begin{pmatrix} -\vec{\sigma}\vec{p}_\mathrm{n}\delta_{\vec{p}_\mathrm{n},\vec{p}_\mathrm{m}} & \sum_{\vec{q}_\mathrm{k}} M^{\pm}_{\vec{q}_\mathrm{k}}\delta_{\vec{p}_\mathrm{m},\vec{p}_\mathrm{n}\pm\vec{q}_\mathrm{k}} \\ \sum_{\vec{q}_\mathrm{k}} M^{\mp}_{\vec{q}_\mathrm{k}}\delta_{\vec{p}_\mathrm{m},\vec{p}_\mathrm{n}\mp\vec{q}_\mathrm{k}} & \vec{\sigma}\vec{p}_\mathrm{n}\delta_{\vec{p}_\mathrm{n},\vec{p}_\mathrm{m}} \end{pmatrix} \tag{C.6}$$

In the penultimate step, we used the representation of the Kronecker delta distribution

$$\int \mathrm{d}^3\vec{x}\; e^{i(\vec{p}_\mathrm{n}-\vec{p}_\mathrm{m})\vec{x}} = V\delta_{\vec{p}_\mathrm{n},\vec{p}_\mathrm{m}} \tag{C.7}$$

and the projectors

$$P_\pm := \frac{1}{2}\left(1\pm\gamma^5\right). \tag{C.8}$$

C.2 Inverse propagator in momentum space

First, we consider the euclidean action

$$\tilde{S}_\mathrm{Euclid} = \int_{V_4}\mathrm{d}^4x\;\left(\mathscr{L}_\mathrm{MF} + \bar{\psi}\mu\gamma^0\psi\right) \tag{C.9}$$

$$= \int_0^{1/T}\mathrm{d}\tau\int\mathrm{d}^3\vec{x}\;\left(\bar{\psi}\underbrace{\gamma^0\left(-\partial_\tau - H(\vec{x})+\mu\right)}_{=:S^{-1}}\psi - \mathscr{V}(\vec{x})\right) \tag{C.10}$$

$$= \tilde{S}_\mathrm{kin} - \tilde{S}_\mathrm{cond} \tag{C.11}$$

with the kinetic and the condensate part $\tilde{S}_\mathrm{kin}$ and $\tilde{S}_\mathrm{cond}$ defined by:

$$\tilde{S}_\mathrm{kin} := \int_0^{1/T}\mathrm{d}\tau\int\mathrm{d}^3\vec{x}\;\left(\bar{\psi}\gamma^0\left(-\partial_\tau - H(\vec{x})+\mu\right)\psi\right) \tag{C.12}$$

$$\tilde{S}_\mathrm{cond} := \int_0^{1/T}\mathrm{d}\tau\int\mathrm{d}^3\vec{x}\;\mathscr{V}(\vec{x}) \tag{C.13}$$

Furthermore, we expand the spinor fields and the condensate in Fourier components in a finite volume V

$$\psi(x) = \frac{1}{\sqrt{V}} \sum_{p_\mathrm{n}} \psi_{p_\mathrm{n}} e^{-ip_\mathrm{n}x} = \frac{1}{\sqrt{V}} \sum_{\omega_\mathrm{n}} \sum_{\vec{p}_\mathrm{n}} \psi_{p_\mathrm{n}} e^{-i(\omega_\mathrm{n}\tau - \vec{p}_\mathrm{n}\vec{x})} \tag{C.14}$$

$$M^{\pm}(\vec{x}) = \sum_{q_\mathrm{k}} M^{\pm}_{q_\mathrm{k}} e^{\mp iq_\mathrm{k}x} = \sum_{\vec{q}_\mathrm{k}} M^{\pm}_{\vec{q}_\mathrm{k}} e^{\pm i\vec{q}_k\vec{x}} \tag{C.15}$$

with

$$M^{+}(\vec{x}) = M(\vec{x}) \tag{C.16}$$

$$M^{-}(\vec{x}) = M^{*}(\vec{x}) \tag{C.17}$$

$$p_\mathrm{n} = (i\omega_\mathrm{n}, \vec{p}_\mathrm{n}) \tag{C.18}$$

$$q_\mathrm{k} = (0, \vec{q}_\mathrm{k}) \tag{C.19}$$

because we assume a static condensate ($q_0 = 0$). Inserting the above Fourier expansion in the kinetic part $\tilde{S}_\mathrm{kin}$, we get:

$$\tilde{S}_\mathrm{kin} = \frac{1}{V} \int_0^{1/T} \mathrm{d}\tau \int \mathrm{d}^3\vec{x} \sum_{\omega_\mathrm{n},\omega_\mathrm{m}} \sum_{\vec{p}_\mathrm{n},\vec{p}_\mathrm{m}} \bar{\psi}_{p_\mathrm{m}} e^{i(\omega_\mathrm{m}\tau - \vec{p}_\mathrm{m}\vec{x})} \gamma^0 \left[-\partial_\tau - \left(H^{+}(\vec{x}) \otimes H^{-}(\vec{x}) \right) + \mu \right] \psi_{p_\mathrm{n}} e^{-i(\omega_\mathrm{n}\tau - \vec{p}_\mathrm{n}\vec{x})} \tag{C.20}$$

$$= \frac{1}{V} \int_0^{1/T} \mathrm{d}\tau \int \mathrm{d}^3\vec{x} \sum_{\omega_\mathrm{n},\omega_\mathrm{m}} \sum_{\vec{p}_\mathrm{n},\vec{p}_\mathrm{m}} \bar{\psi}_{p_\mathrm{m}} e^{i(\omega_\mathrm{m}\tau - \vec{p}_\mathrm{m}\vec{x})} \gamma^0 \left[i\omega_\mathrm{n} - \left(H^{+}(\vec{x}) \otimes H^{-}(\vec{x}) \right) + \mu \right] \psi_{p_\mathrm{n}} e^{-i(\omega_\mathrm{n}\tau - \vec{p}_\mathrm{n}\vec{x})} \tag{C.21}$$

The Fourier transformation of the Hamiltonian in C.1 and the representation of the Kronecker delta distribution in the time component

$$\int_0^{1/T} \mathrm{d}\tau \; e^{i(\omega_\mathrm{m} - \omega_\mathrm{n})\tau} = \frac{1}{T} \delta_{\omega_\mathrm{m},\omega_\mathrm{n}} \tag{C.22}$$

yields

$$\tilde{S}_\mathrm{kin} = \frac{1}{T} \sum_{\omega_\mathrm{n},\omega_\mathrm{m}} \sum_{\vec{p}_\mathrm{n},\vec{p}_\mathrm{m}} \bar{\psi}_{p_\mathrm{m}} \underbrace{\delta_{\omega_\mathrm{n},\omega_\mathrm{m}} \gamma^0 \left[i\omega_\mathrm{n} \delta_{\vec{p}_\mathrm{n},\vec{p}_\mathrm{m}} - \left(H^{+}_{\vec{p}_\mathrm{m},\vec{p}_\mathrm{n}} \otimes H^{-}_{\vec{p}_\mathrm{m},\vec{p}_\mathrm{n}} \right) + \mu \delta_{\vec{p}_\mathrm{n},\vec{p}_\mathrm{m}} \right]}_{=: S^{-1}_{p_\mathrm{m},p_\mathrm{n}}} \psi_{p_\mathrm{n}} \tag{C.23}$$

$$= \frac{1}{T} \sum_{p_\mathrm{n},p_\mathrm{m}} \bar{\psi}_{p_\mathrm{m}} S^{-1}_{p_\mathrm{m},p_\mathrm{n}} \psi_{p_\mathrm{n}} \tag{C.24}$$

with

$$H^{\pm}_{\vec{p}_\mathrm{m},\vec{p}_\mathrm{n}} = \gamma^0 \vec{\gamma} \vec{p}_\mathrm{n} \delta_{\vec{p}_\mathrm{n},\vec{p}_\mathrm{m}} + \sum_{\vec{q}_\mathrm{k}} M^{\pm}_{\vec{q}_\mathrm{k}} \delta_{\vec{p}_\mathrm{m},\vec{p}_\mathrm{n} \pm \vec{q}_\mathrm{k}} \gamma^0 P_{+} + \sum_{\vec{q}_\mathrm{k}} M^{\mp}_{\vec{q}_\mathrm{k}} \delta_{\vec{p}_\mathrm{m},\vec{p}_\mathrm{n} \mp \vec{q}_\mathrm{k}} \gamma^0 P_{-} \,. \tag{C.25}$$

D Calculation of the kinetic part of the thermodynamic potential

For the kinetic part of the thermodynamic potential, we have to calculate

$$\Omega_\mathrm{kin} = -\frac{T}{V} \; \mathrm{Tr} \left[\ln \left(\frac{S^{-1}}{T} \right) \right]. \tag{D.1}$$

The trace over the flavor and color space and the representation of the inverse propagator S^{-1} in the momentum space (see C.2) yields

$$\Omega_{\text{kin}} = -\frac{T}{V} N_{\text{f}} N_{\text{c}} \sum_n \text{tr}_{\text{Dirac},\vec{p}} \left[\ln\left(\frac{1}{T} \gamma^0 \left(i\omega_{\text{n}} - H_{\vec{p}} + \mu \right) \right) \right]. \tag{D.2}$$

Using $\text{tr} \ln M = \ln \det M$ and $\det \gamma^0 = 1$, we can get rid of the γ^0 matrix:

$$\Omega_{\text{kin}} = -\frac{T}{V} N_{\text{f}} N_{\text{c}} \sum_n \text{tr}_{\text{Dirac},\vec{p}} \left[\ln\left(\frac{1}{T} \left(i\omega_{\text{n}} - H_{\vec{p}} + \mu \right) \right) \right] \tag{D.3}$$

Furthermore, using the fact that the Hamiltonian is a hermitian operator, we denote the eigenstates and the eigenvalues of $H_{\vec{p}}$ in Dirac and momentum space with E_λ:

$$\Omega_{\text{kin}} = -\frac{T}{V} N_{\text{f}} N_{\text{c}} \sum_{E_\lambda} \sum_n \ln\left(\frac{1}{T} \left(i\omega_{\text{n}} - E_\lambda + \mu \right) \right) \tag{D.4}$$

In the next step, we will employ the Matsubara formalism [21]. One can write the sum over the Matsubara frequencies as an integral over the contour Γ_1 (see fig. D.1) performing the residue theorem (another possibility is to perform the sum directly, see appendix D.1)

$$\Omega_{\text{kin}} = -\frac{T}{V} N_{\text{f}} N_{\text{c}} \sum_{E_\lambda} \sum_n \ln\left(\frac{1}{T} \left(i\omega_{\text{n}} - E_\lambda + \mu \right) \right) \tag{D.5}$$

$$= -\frac{1}{V} N_{\text{f}} N_{\text{c}} \sum_{E_\lambda} \int_{\Gamma_1} \frac{\text{d}z}{2\pi i} \ln\left(\frac{z - E_\lambda + \mu}{T} \right) n_{\text{F}}(-z) \tag{D.6}$$

with $i\omega_n = (2n+1)\pi i T$ and the Fermi distribution function $n_{\text{F}}(z) = (1 + \exp(z/T))^{-1}$. The poles of $n_{\text{F}}(z)$ are the Matsubara frequencies and the residue are given by $\text{Res}(n_{\text{F}}(\pm z), i\omega_n) = \mp T$. Since the logarithm has a branch cut on the negative real axis, we deform the integration contour Γ_1 to Γ_2 (fig. D.1) around $-\infty < z \leq E_\lambda - \mu$. It follows:

$$\Omega_{\text{kin}} = -\frac{1}{V} N_{\text{f}} N_{\text{c}} \sum_{E_\lambda} \int_{-\infty}^{E_\lambda - \mu} \frac{\text{d}z}{2\pi i} \left[\ln\left(\frac{z + i\epsilon - E_\lambda + \mu}{T} \right) n_{\text{F}}(-z + i\epsilon) - \ln\left(\frac{z - i\epsilon - E_\lambda + \mu}{T} \right) n_{\text{F}}(-z - i\epsilon) \right] \tag{D.7}$$

Dropping the infinitesimal ϵ term in the Fermi distribution function, since the branch cut appears only in the logarithm and using the relations

$$\ln(z) = \ln(|z|) + i\text{Arg}(z) \tag{D.8}$$

$$\text{Arg}(z^*) = -\text{Arg}(z)\,, \tag{D.9}$$

we can integrate the above expression analytically:

$$\Omega_{\text{kin}} = -\frac{T}{V} N_{\text{f}} N_{\text{c}} \sum_{E_\lambda} \ln\left[2\cosh\left(\frac{E_\lambda - \mu}{2T} \right) \right] = -\frac{T}{V} N_{\text{f}} N_{\text{c}} \sum_{E_\lambda} \left[\frac{E_\lambda - \mu}{2T} + \ln\left(1 + \exp\left(-\frac{E_\lambda - \mu}{T} \right) \right) \right] \tag{D.10}$$

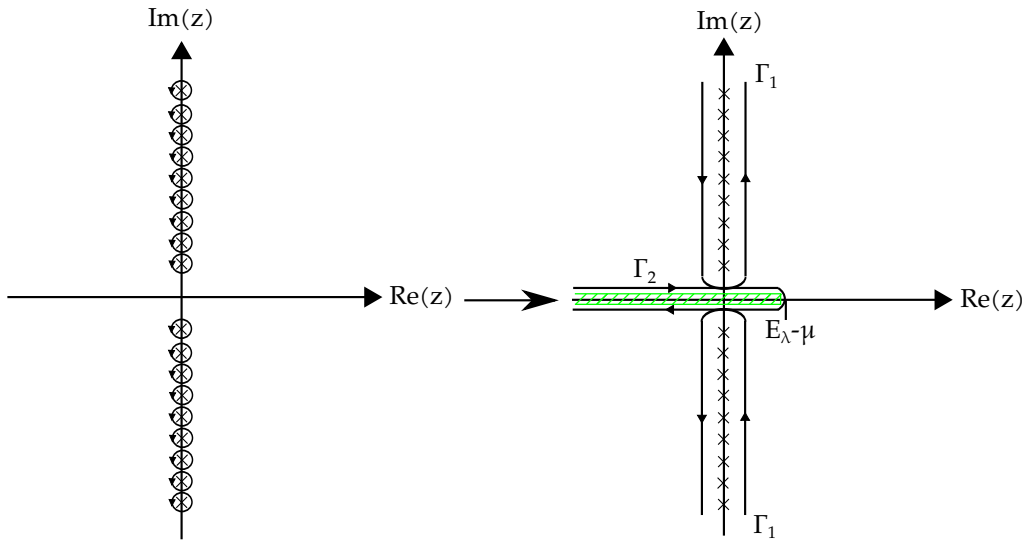

Figure D.1: Integration contour of the kinetic part of the thermodynamic potential Ω_{kin}: The circles around the Matsubara frequencies are merged to Γ_1. Then the integration contour Γ_1 is deformed to the integration contour Γ_2 around the branch cut of the logarithm (dashed region).

D.1 Matsubara relation

We start with the Matsubara sum:

$$\sum_{n=-\infty}^{\infty} \ln\left[\frac{i\omega_{\text{n}}-(E_\lambda-\mu)}{T}\right] = \frac{1}{2}\sum_{n=-\infty}^{\infty} \ln\left[\frac{\omega_{\text{n}}^2+(E_\lambda-\mu)^2}{T^2}\right] = \frac{1}{2}\sum_{n=-\infty}^{\infty} \ln\left[(2n+1)^2\pi^2+\frac{(E_\lambda-\mu)^2}{T^2}\right] \tag{D.11}$$

$$\overset{\theta=(E_\lambda-\mu)/T}{=} \frac{1}{2}\sum_{n=-\infty}^{\infty} \ln\left[(2n+1)^2\pi^2+\theta^2\right] \tag{D.12}$$

Here, we can first derive the sum with respect to θ and then sum up the expression:

$$\sum_{n=-\infty}^{\infty} \frac{\partial}{\partial\theta}\ln\left[(2n+1)^2\pi^2+\theta^2\right] = \sum_{n=-\infty}^{\infty} \frac{2\theta}{(2n+1)^2\pi^2+\theta^2} = \tanh\left(\frac{\theta}{2}\right) \tag{D.13}$$

$$\Longrightarrow \sum_{n=-\infty}^{\infty} \ln\left[(2n+1)^2\pi^2+\theta^2\right] = \int \tanh\left(\frac{\theta}{2}\right)\mathrm{d}\theta = 2\ln\left[\cosh\left(\frac{\theta}{2}\right)\right]+\text{const} \tag{D.14}$$

$$= -2\ln(2)+\theta+2\ln\left(1+e^{-\theta}\right)+\text{const} \tag{D.15}$$

Since the constant terms do not depend on the temperature and the chemical potential, we can drop these:

$$\sum_{n=-\infty}^{\infty} \ln\left[(2n+1)^2\pi^2+\theta^2\right] = \theta+2\ln\left(1+e^{-\theta}\right) = 2\ln\left[2\cosh\left(\frac{\theta}{2}\right)\right] \tag{D.16}$$

Inserting this relation in (D.12), we get

$$\sum_{n=-\infty}^{\infty} \ln\left[\frac{i\omega_{\text{n}}-(E_\lambda-\mu)}{T}\right] = \ln\left[2\cosh\left(\frac{E_\lambda-\mu}{2T}\right)\right] \tag{D.17}$$

and finally the kinetic part of the thermodynamic potential

$$\Omega_{\text{kin}} = -\frac{T}{V} N_{\text{f}} N_{\text{c}} \sum_{E_\lambda} \ln\left[2\cosh\left(\frac{E_\lambda - \mu}{2T}\right)\right] = -\frac{T}{V} N_{\text{f}} N_{\text{c}} \sum_{E_\lambda} \left[\frac{E_\lambda - \mu}{2T} + \ln\left(1 + \exp\left(-\frac{E_\lambda - \mu}{T}\right)\right)\right]. \quad \text{(D.18)}$$

E Asymptotic spectral density

For high energies, the kinetic part of the thermodynamic potential can be approximated with an integral over the asymptotic density of states [17] given by

$$\rho_{\text{A}}(E) = \frac{E^2}{\pi^2} - \frac{\langle |M(z)|^2 \rangle}{2\pi^2} - \frac{\langle |M(z)|^4 \rangle + \langle |M'(z)|^2 \rangle}{8\pi^2 E^2} + \mathcal{O}(E^{-4}) \,. \quad \text{(E.1)}$$

Hence, we split the kinetic part of the thermodynamic potential as follows:

$$\Omega_{\text{kin}} \approx \Omega_{\text{kin}}^{\Lambda_{\text{E}}} + \Omega_{\text{kin}}^{\text{A}}$$

with

$$\begin{aligned}
\Omega_{\text{kin}}^{\Lambda_{\text{E}}} = &-\frac{N_{\text{c}} N_{\text{f}}}{(2\pi)^2} \int_0^q \mathrm{d}k_{\text{z}} \int_0^\infty \mathrm{d}p_\perp \, p_\perp \times \\
&\times \sum_{\lambda_{\text{BdG}}} \left\{ \sum_{j=0}^{3} c_j \cdot \sqrt{\lambda_{\text{BdG}}^2 + p_\perp^2 + j\Lambda^2} + T \sum_{s\in\{-1,1\}} \ln\left[1 + \exp\left(-\frac{\sqrt{\lambda_{\text{BdG}}^2 + p_\perp^2} - s\mu}{T}\right)\right] \right\} \times \\
&\times \theta\left(\Lambda_{\text{E}} - \sqrt{\lambda_{\text{BdG}}^2 + p_\perp^2}\right) \qquad \text{(E.2)} \\
\Omega_{\text{kin}}^{\text{A}} = &-N_{\text{c}} N_{\text{f}} \int_{\Lambda_{\text{E}}}^\infty \mathrm{d}E \; \rho_{\text{A}}(E) \cdot \left\{ \sum_{j=0}^{3} c_j \cdot \sqrt{E^2 + j\Lambda^2} + T \sum_{s\in\{-1,1\}} \ln\left[1 + \exp\left(-\frac{E - s\mu}{T}\right)\right] \right\}. \qquad \text{(E.3)}
\end{aligned}$$

The diagonalization procedure of the Hamilton matrix requires a numerical cutoff in momentum space, which leads to boundary effects. To take account of these, we implement the matrix with an asymptotic cutoff $\Lambda_{\text{A}} \approx 12$ GeV and sort out the boosted eigenvalues by the cutoff $\Lambda_{\text{E}} = \Lambda_{\text{A}} - \Delta E$ in the Heaviside step function in $\Omega_{\text{kin}}^{\Lambda_{\text{E}}}$ (eq. (E.2)). The energy difference ΔE has to be chosen that the boundary effects are negligible. In our numerical calculations ΔE lies between 1 GeV and 2 GeV.
Like in (4.17), the integration over $p_\perp$ in (E.2) yields

$$\Omega_{\text{kin}}^{\Lambda_{\text{E}}} = -\frac{N_{\text{c}} N_{\text{f}}}{(2\pi)^2} \int_0^q \mathrm{d}k_{\text{z}} \sum_{\lambda_{\text{BdG}}} \left[f_{\text{PV}}(\lambda_{\text{BdG}}) + f_{\text{med}}(\lambda_{\text{BdG}}; T, \mu)\right] \cdot \theta\left(\Lambda_{\text{E}} - |\lambda_{\text{BdG}}|\right) \quad \text{(E.4)}$$

with

$$f_{\text{PV}}(\lambda_{\text{BdG}}) := \sum_{j=0}^{3} \frac{c_j}{3} \cdot \left[\left(\Lambda_{\text{E}}^2 + j\Lambda^2\right)^{3/2} - \left(\lambda_{\text{BdG}}^2 + j\Lambda^2\right)^{3/2}\right] \quad \text{(E.5)}$$

$$\begin{aligned}
f_{\text{med}}(\lambda_{\text{BdG}}; T, \mu) := T^2 \sum_{s\in\{-1,1\}} \Big[&\Lambda_{\text{E}} \cdot \text{Li}_2\left(-e^{-\frac{1}{T}(\Lambda_{\text{E}} - s\mu)}\right) + T\,\text{Li}_3\left(-e^{-\frac{1}{T}(\Lambda_{\text{E}} - s\mu)}\right) \\
&- |\lambda_{\text{BdG}}| \cdot \text{Li}_2\left(-e^{-\frac{1}{T}(|\lambda_{\text{BdG}}| - s\mu)}\right) - T\,\text{Li}_3\left(-e^{-\frac{1}{T}(|\lambda_{\text{BdG}}| - s\mu)}\right)\Big] \qquad \text{(E.6)}
\end{aligned}$$

$$\begin{aligned}
f_{\text{med}}(\lambda_{\text{BdG}}; T = 0, \mu) := &\frac{1}{6} \sum_{s\in\{-1,1\}} \theta(s\mu - \Lambda_{\text{E}}) \cdot \left[s\mu\left(\mu^2 - 3\Lambda_{\text{E}}^2\right) + 2\Lambda_{\text{E}}^3\right] \\
&- \theta(s\mu - |\lambda_{\text{BdG}}|) \cdot \left[s\mu\left(\mu^2 - 3\lambda_{\text{BdG}}^2\right) + 2|\lambda_{\text{BdG}}|^3\right]. \qquad \text{(E.7)}
\end{aligned}$$

The expectation values in the asymptotic spectral density can be calculated by inserting the mass ansatz (2.34) in (E.1):

$$\langle |M(z)|^2 \rangle = \frac{1}{L} \int_0^L \mathrm{d}z \; |M(z)|^2 = \sum_n |M_n|^2 \tag{E.8}$$

$$\langle |M'(z)|^2 \rangle = \frac{1}{L} \int_0^L \mathrm{d}z \; |M'(z)|^2 = q^2 \cdot \sum_n n^2 |M_n|^2 \tag{E.9}$$

$$\langle |M(z)|^4 \rangle = \frac{1}{L} \int_0^L \mathrm{d}z \; |M(z)|^4 = \sum_{n_1,n_2,n_3,n_4} M_{n_1} M_{n_3} M^*_{n_2} M^*_{n_4} \delta_{n_1+n_3,n_2+n_4} \tag{E.10}$$

where $L = 2\pi/q$ is the size of the Wigner-Seitz cell. The same asymptotic procedure can be applied on the gap equations

$$M_n - m\delta_{n,0} = 4 g_\mathrm{s} N_\mathrm{f} N_\mathrm{c} \cdot \left(g^{\Lambda_\mathrm{E}} + g^\mathrm{A} \right) \tag{E.11}$$

$$\tag{E.12}$$

where g^{Λ_E} is the numerical diagonalization part

$$\begin{aligned} g^{\Lambda_\mathrm{E}} := \frac{-1}{(2\pi)^2} \int_0^q \mathrm{d}k_\mathrm{z} \sum_{\lambda_\mathrm{BdG}} \lambda_\mathrm{BdG} \frac{\partial \lambda_\mathrm{BdG}}{\partial M^*_n} \cdot \theta\left(\Lambda_\mathrm{E} - |\lambda_\mathrm{BdG}|\right) \times \\ \times \left\{ \sum_{j=0}^{3} c_j \left(\lambda^2_\mathrm{BdG} + j\Lambda^2 \right) + T \sum_{s\in\{-1,1\}} \ln\left[1 + \exp\left(-\frac{1}{T} \left(|\lambda_\mathrm{BdG}| - s\mu \right) \right) \right] \right\} \end{aligned} \tag{E.13}$$

and the asymptotic part

$$g^\mathrm{A} := \int_{\Lambda_\mathrm{E}}^\infty \mathrm{d}E \; \frac{\partial \rho_\mathrm{A}(E)}{\partial M^*_n} \cdot \left\{ \sum_{j=0}^{3} c_j \cdot \sqrt{E^2 + j\Lambda^2} + T \sum_{s\in\{-1,1\}} \ln\left[1 + \exp\left(-\frac{E - s\mu}{T} \right) \right] \right\} \tag{E.14}$$

with

$$\frac{\partial \rho_\mathrm{A}(E)}{\partial M^*_n} = -\frac{M_n}{2\pi^2} - \frac{1}{8\pi^2 E^2} \cdot \left(q^2 n^2 \cdot M_n + 2 \sum_{n_1,n_2,n_3} M_{n_1} M_{n_3} M^*_{n_2} \delta_{n_1+n_3,n+n_2} \right) + \mathcal{O}(E^{-4}). \tag{E.15}$$

Note, the used asymptotic spectral density (E.1) differs from [17] in matters of the expectation values. The derivation was made for real order parameter. Since we consider a complex modulation, we take the absolute value of $M(z)$. Nevertheless, the first term E^2/π^2, which corresponds to non-interacting massless particles (ultra-relativistic gas), is independent of the expectation values and has the largest impact on the behavior of the density of states for high energies.

F Derivation of the CDW gap equation

To obtain analytic eigenvalues we follow [19] and analyze the structure of the Hamiltonian with the first Fourier component:

$$H^{\mathrm{BdG},+} = \begin{pmatrix} \ddots & & & & & \\ & p_j & 0 & 0 & 0 & 0 \\ & 0 & \begin{bmatrix} -p_j & M_1 \\ M_1 & p_{j-1} \end{bmatrix} & \mathbf{0} & \mathbf{0} & 0 \\ & 0 & \mathbf{0} & \begin{bmatrix} -p_{j-1} & M_1 \\ M_1 & P_{j-2} \end{bmatrix} & \mathbf{0} & 0 \\ & 0 & \mathbf{0} & \mathbf{0} & \begin{bmatrix} -p_{j-2} & M_1 \\ M_1 & p_{j-3} \end{bmatrix} & 0 \\ & 0 & 0 & 0 & 0 & -p_{j-3} \\ & & & & & \ddots \end{pmatrix} \tag{F.1}$$

The momenta p_j are given by:

$$p_j = k_z + jq, \quad j \in \mathbb{Z} \tag{F.2}$$

Since we introduce a numerical cutoff the edge momenta entries can be neglected. Then, the Hamiltonian exhibits a block diagonal structure with the 2×2 blocks defined by

$$B_j = \begin{bmatrix} -p_j & M_1 \\ M_1 & p_{j-1} \end{bmatrix}. \tag{F.3}$$

The eigenvalues of each block can be calculated analytically

$$\lambda_j^{\pm} = \frac{q}{2} \pm \sqrt{\left(p_j + \frac{q}{2}\right)^2 + M_1^2} \tag{F.4}$$

$$= \frac{q}{2} \pm \sqrt{\tilde{p}_j^2 + M_1^2} \tag{F.5}$$

where we redefined the block momenta to $\tilde{p}_j = k_z + jq/2$. Inserting these momenta into equation (4.17), we see that the integration over the Brillouin zone times the sum of all block eigenvalues can be expanded over the whole one-dimensional momentum space

$$\Omega_{\mathrm{kin}} = \frac{N_c N_f}{(2\pi)^2} \int_0^q \mathrm{d}k_z \sum_{n=-\infty}^{\infty} \left[\tilde{f}\left(|\lambda_n^+(k_z)|\right) + \tilde{f}\left(|\lambda_n^-(k_z)|\right)\right] \tag{F.6}$$

$$= \frac{N_c N_f}{(2\pi)^2} \int_{-\infty}^{\infty} \mathrm{d}k_z \left[\tilde{f}\left(|\lambda_{\mathrm{CDW}}^+(k_z)|\right) + \tilde{f}\left(|\lambda_{\mathrm{CDW}}^-(k_z)|\right)\right] \tag{F.7}$$

with the integrand

$$\tilde{f}\left(|\lambda_{\mathrm{CDW}}^{\pm}|\right) = \tilde{f}_{\mathrm{vac,PV}}\left(|\lambda_{\mathrm{CDW}}^{\pm}|\right) + \tilde{f}_{\mathrm{med}}\left(|\lambda_{\mathrm{CDW}}^{\pm}|\right) \tag{F.8}$$

$$\tilde{f}_{\mathrm{vac,PV}}\left(|\lambda_{\mathrm{CDW}}^{\pm}|\right) = \sum_{j=0}^{3} \frac{c_j}{3} \cdot \left[\left(\lambda_{\mathrm{CDW}}^{\pm}\right)^2 + j\Lambda^2\right]^{3/2} \tag{F.9}$$

$$\tilde{f}_{\mathrm{med}}\left(|\lambda_{\mathrm{CDW}}^{\pm}|\right) = \sum_{s\in\{-1,1\}} \begin{cases} T^2\left[|\lambda_{\mathrm{CDW}}^{\pm}| \cdot \mathrm{Li}_2\left(-e^{-\frac{1}{T}\left(|\lambda_{\mathrm{CDW}}^{\pm}| - s\mu\right)}\right) + T\,\mathrm{Li}_3\left(-e^{-\frac{1}{T}\left(|\lambda_{\mathrm{CDW}}^{\pm}| - s\mu\right)}\right)\right] & \text{if } T > 0 \\ \frac{1}{6}\theta\left(s\mu - |\lambda_{\mathrm{CDW}}^{\pm}|\right) \cdot \left[s\mu\left(\mu^2 - 3\left(\lambda_{\mathrm{CDW}}^{\pm}\right)^2\right) + 2|\lambda_{\mathrm{CDW}}^{\pm}|^3\right] & \text{if } T = 0 \end{cases} \tag{F.10}$$

and the continuous eigenvalues

$$\lambda^{\pm}_{\mathrm{CDW}}(k_z) = \sqrt{k_z^2 + M_1^2} \pm \frac{q}{2}. \tag{F.11}$$

The gap equation follows immediately from the derivative of the full thermodynamic potential $\Omega = \Omega_{\mathrm{kin}} + \Omega_{\mathrm{cond}}$ with respect to M_1:

$$M_1 = -\frac{2N_c N_f}{(2\pi)^2} g_s M_1 \int_{-\infty}^{\infty} \mathrm{d}k_z \frac{1}{\sqrt{k_z^2 + M_1^2}} \left[\lambda^{+}_{\mathrm{CDW}}(k_z) \cdot \tilde{g}\left(\lambda^{+}_{\mathrm{CDW}}(k_z)\right) + \lambda^{-}_{\mathrm{CDW}}(k_z) \cdot \tilde{g}\left(\lambda^{-}_{\mathrm{CDW}}(k_z)\right) \right] \tag{F.12}$$

with

$$\tilde{g}(\lambda^{\pm}_{\mathrm{CDW}}) = \sum_{j=0}^{3} c_j \cdot \sqrt{(\lambda^{\pm}_{\mathrm{CDW}})^2 + j\Lambda^2} + \sum_{s\in\{-1,1\}} \begin{cases} T \ln\left[1 + \exp\left(-\frac{|\lambda^{\pm}_{\mathrm{CDW}}| - s\mu}{T}\right)\right] & \text{if } T > 0 \\ \theta\left(s\mu - |\lambda^{\pm}_{\mathrm{CDW}}|\right) \cdot \left(s\mu - |\lambda^{\pm}_{\mathrm{CDW}}|\right) & \text{if } T = 0 \end{cases}. \tag{F.13}$$

References

[1] H. Fritzsch, M. Gell-Mann, and H.Leutwyler. Advantages of the color octet gluon picture. *Phys. Lett. B47: 365-368*, 1973.

[2] D. J. Gross. Twenty five years of asymptotic freedom. *Nucl.Phys.Proc.Suppl. 74:426-446*, 1999. arXiv:hep-th/9809060v1.

[3] F. Wilczek. Asymptotic freedom: From paradox to paradigm . *Proc.Nat.Acad.Sci.102:8403-8413; Int.J.Mod.Phys.A20:5753-5778; Rev.Mod.Phys.77:857-870*, 2005. arXiv:hep-ph/0502113v2.

[4] D. J. Gross and F. Wilczek. Ultraviolet behavior of non-abelian gauge theories. *Phys. Rev. Lett. 30, 1343*, 1973.

[5] H. D. Politzer. Reliable perturbative results for strong interactions? *Phys. Rev. Lett. 30, 1346*, 1973.

[6] D. G. Richards. Lattice gauge theory- QCD from quarks to hadrons. 2000. arXiv:nucl-th/0006020v2.

[7] M. A. Stephanov. QCD phase diagram: an overview. *PoS LAT2006:024*, 2006.

[8] K. Fukushima and T. Hatsuda. The phase diagram of dense QCD. *Rept.Prog.Phys.74:014001*, 2011.

[9] M. G. Alford, K. Rajagopal, T. Schaefer, and A. Schmitt. Color superconductivity in dense quark matter. *Rev.Mod.Phys.80:1455-1515*, 2008.

[10] A. W. Overhauser. Structure of Nuclear Matter. *Phys. Rev. 4, 415*, 1960.

[11] P. Fulde and R. A. Ferrell. Superconductivity in a strong spin-exchange field. *Phys. Rev. 135, A550*, 1964.

[12] A. I. Larkin and Y. N. Ovchinnikov. Nonuniform state of superconductors. *Zh.Eksp.Teor.Fiz. 47 1136*, 1964.

[13] Y. Nambu and G. Jona-Lasinio. Dynamical model of elementary particles based on an analogy with superconductivity. i. *Phys. Rev. 122, 345-358*, 1961.

[14] Y. Nambu and G. Jona-Lasinio. Dynamical model of elementary particles based on an analogy with superconductivity. ii. *Phys. Rev. 124, 246-254*, 1961.

[15] M. Gell-Mann and M. Levy. The axial vector current in beta decay. *Nuovo Cim. 16 (1960) 705*, 1960.

[16] O. Scavenius, A. Mocsy, I.N. Mishustin, and D.H. Rischke. Chiral phase Transition within effective models with constituent quarks. *Phys.Rev.C64:045202*, 2001.

[17] D. Nickel. Inhomogeneous phases in the Nambu–Jona-Lasinio and quark-meson model. *PhysRevD.80.074025*, 2009. arXiv:0906.5295v1.

[18] M. Buballa and S. Carignano. Inhomogeneous chiral condensates. *Prog.Part.Nucl.Phys. 81, 39-96*, 2015.

[19] S. Carignano. *Inhomogeneous chiral symmetry breaking phases*. PhD thesis, Institut für Kernphysik. Technische Universität Darmstadt, 2012. URL: http://tuprints.ulb.tu-darmstadt.de/3149/1/thesis_carignano.pdf.

[20] URL: https://www-alt.gsi.de/forschung/fair_experiments/CBM/Phasendiagram.jpg.

[21] J. I. Kapusta and C. Gale. *Finite-Temperature Field Theory. Principles and Applications.* Cambridge University Press, 2nd edition, 2006.

[22] F. Bloch. Über die Quantenmechanik der Elektronen in Kristallgittern. *Zeitschrift für Physik A Hadrons and Nuclei, 52(7):555-600.*, 1929.

[23] M. Buballa and D. Nickel. Solitonic ground states in (color-)superconductivity. *Phys.Rev.D79:054009*, 2009. arXiv:0811.2400v2.

[24] J.A. Nelder and R. Mead. A Simplex Method for Function Minimization. *Computer Journal 7 308-313*, 1965.

[25] H. G. A. Hellmann. *Einführung in die Quantenchemie*. F. Deuticke, Leipzig, 1937.

[26] R. P. Feynman. Forces in Molecules. *Phys. Rev. 56, 340*, 1939.

[27] W. Pauli and E. Villars. On the invariant regularization in relativistic quantum theory. *Rev. Mod. Phys., 21(3):434-444*, 1949.

[28] S. P. Klevansky. The Nambu-Jona-Lasinio model of quantum chromodynamics. *Rev. Mod. Phys., 64(3):649-708*, 1992.

[29] J. Gasser and H. Leutwyler. Low energy theorems as precision tests of QCD. *Physics Letters B 125 no. 4*, 1983.

[30] M. Galassi et al. *GNU Scientific Library Reference Manual*. Third edition. URL: http://www.gnu.org/software/gsl/.

[31] G. Basar and G. V. Dunne. A Twisted Kink Crystal in the Chiral Gross-Neveu model. *Phys.Rev.D78:065022*, 2008. arXiv:0806.2659v2.

[32] L. P. Pitaevskii S. Giorgini and S. Stringari. Theory of ultracold Fermi gases. *Rev. Mod. Phys. 80, 1215*, 2008.

[33] G. V. Dunne F. Correa and M. S. Plyushchay. The Bogoliubov/de Gennes system, the AKNS hierarchy, and nonlinear quantum mechanical supersymmetry. *Annals Phys.324:2522-2547*, 2009. arXiv:0904.2768v2.

[34] E. Anderson, Z. Bai, C. Bischof, S. Blackford, J. Demmel, J. Dongarra, J. Du Croz, A. Greenbaum, S. Hammarling, A. McKenney, and D. Sorensen. *LAPACK Users' Guide*. Society for Industrial and Applied Mathematics, Philadelphia, PA, third edition, 1999.

[35] M. Schramm. Inhomogeneous Phases in the Vector Interaction Extended Nambu–Jona-Lasinio Model. Master's thesis, Institut für Kernphysik. Technische Universität Darmstadt, 2013. URL: http://theorie.ikp.physik.tu-darmstadt.de/nhq/downloads/thesis/master.schramm.pdf.

[36] M. Thies O. Schnetz and R. K. Urlichs. Full Phase Diagram of the Massive Gross-Neveu Model. *AnnalsPhys.321:2604-2637*, 2006. arXiv:hep-th/0511206v2.

[37] D. Ishibashi H. Abuki and K. Suzuki. Crystalline chiral condensates off the tricritical point in a generalized Ginzburg-Landau approach. *Phys.Rev.D85:074002*, 2012. arXiv:1109.1615v3.

[38] M. Schramm. Private communication, 2016.

[39] G. Ecker. Quantum chromodynamics. 2006. arXiv:hep-ph/0604165v1.

[40] U. Vogl and W. Weise. The Nambu and Jona-Lasinio model: Its implications for hadrons and nuclei. *Prog. Part. Nucl. Phys., 27:195-272*, 1991.

[41] V. Koch. Aspects of chiral symmetry. *Int.J.Mod.Phys. E6:203-250*, 1997. arXiv:nucl-th/9706075v2.

[42] M. E. Peskin and D. V. Schröder. *An Introduction To Quantum Field Theory*. Perseus Books, 1995.

[43] J. Hirsch. Mesonic Excitations in an Inhomogeneous Phase of the Nambu–Jona-Lasinio Model. Master's thesis, Institut für Kernphysik. Technische Universität Darmstadt, 2013. URL: http://theorie.ikp.physik.tu-darmstadt.de/nhq/downloads/thesis/master.hirsch.pdf.

[44] S. Möller. Pion-Pion scattering and shear viscosity in the Nambu–Jona-Lasinio model. Master's thesis, Institut für Kernphysik. Technische Universität Darmstadt, 2012. URL: http://theorie.ikp.physik.tu-darmstadt.de/nhc/pages/thesis/master.moeller.pdf.

[45] K. Heckmann. Die Scherviskosität im Nambu-Jona-Lasinio-Modell. Diplomarbeit, Institut für Kernphysik. Technische Universität Darmstadt, 2007. URL: http://crunch.ikp.physik.tu-darmstadt.de/nhc/pages/thesis/diplom.heckmann.pdf.

[46] D. Nowakowski. Inhomogeneous phases and color superconductivity in the NJL model. Master's thesis, Institut für Kernphysik. Technische Universität Darmstadt, 2012. URL: http://theorie.ikp.physik.tu-darmstadt.de/nhq/downloads/thesis/master.nowakowski.pdf.

[47] M. Buballa. NJL-model analysis of dense quark matter. *Phys.Rept. 407:205-376*, 2005. arXiv:hep-ph/0402234v2.

[48] K. G. Wilson. Confinement of quarks. *Phys. Rev. D, 10:2445-2459*, 1974.

[49] E. Nakano and T. Tatsumi. Chiral symmetry and density wave in quark matter. *Phys.Rev.D71:114006*, 2005. arXiv:hep-ph/0411350v5.